APS physics

CHORUS

This is the accepted manuscript made available via CHORUS. The article has been published as:

Triangles bridge the scales: Quantifying cellular contributions to tissue deformation

Matthias Merkel, Raphaël Etournay, Marko Popović, Guillaume Salbreux, Suzanne Eaton, and Frank Jülicher

Phys. Rev. E **95**, 032401 — Published 1 March 2017

DOI: 10.1103/PhysRevE.95.032401

Triangles bridge the scales: Quantifying cellular contributions to tissue deformation

Matthias Merkel,[1,2,*] Raphaël Etournay,[3,4] Marko Popović,[1]
Guillaume Salbreux,[1,5] Suzanne Eaton,[3] and Frank Jülicher[1,†]

[1] *Max Planck Institute for the Physics of Complex Systems, Nöthnitzer Str. 8, 01187 Dresden, Germany*
[2] *Department of Physics, Syracuse University, Syracuse, New York 13244, USA*
[3] *Max Planck Institute of Molecular Cell Biology and Genetics, Pfotenhauerstr. 108, 01307 Dresden, Germany*
[4] *Unité de Génétique et Physiologie de l'Audition, Institut Pasteur, 75015 Paris, France*
[5] *Francis Crick Institute, Lincoln's Inn Fields Laboratory, 44 Lincoln's Inn Fields, London WC2A 3LY, UK*

(Dated: February 2, 2017)

In this article, we propose a general framework to study the dynamics and topology of cellular networks that capture the geometry of cell packings in two-dimensional tissues. Such epithelia undergo large-scale deformation during morphogenesis of a multicellular organism. Large-scale deformations emerge from many individual cellular events such as cell shape changes, cell rearrangements, cell divisions, and cell extrusions. Using a triangle-based representation of cellular network geometry, we obtain an exact decomposition of large-scale material deformation. Interestingly, our approach reveals contributions of correlations between cellular rotations and elongation as well as cellular growth and elongation to tissue deformation. Using this Triangle Method, we discuss tissue remodeling in the developing pupal wing of the fly *Drosophila melanogaster*.

Keywords: cellular material; epithelium; foam; deformation; pure shear; cell shape; T1 transition; cell division; cell extrusion

CONTENTS

I. Introduction 2

II. Polygonal and triangular networks 3
- A. Description of epithelia as a network of polygons 3
- B. Triangulation of a polygonal network 3
- C. The deformation tensor 4
- D. Triangle-based characterization of network deformation 4

III. Triangle shapes and network deformation 6
- A. Shape and orientation of a single triangle 6
- B. Triangle deformations corresponding to triangle shape changes 6
- C. Large-scale deformation of a triangular network 7
  1. Pure shear deformation on large scales 7
  2. Elongation and shear of a single cell 8
  3. Isotropic expansion on large scales 8

IV. Contributions of topological transitions to network deformation 9
- A. Contribution of a single topological transition to pure shear 9
- B. Contribution of a single topological transition to isotropic expansion 10

V. Cellular contributions to the large-scale deformation rate 11
- A. Pure shear rate 11
- B. Isotropic expansion rate 11
- C. Cumulative shear and expansion 11

VI. Tissue remodeling in the pupal fly wing as an example 11

VII. Discussion 15

Acknowledgements 16

A. Deformation of a triangle network 16
- 1. Deformation and deformation gradients 16
- 2. Triangulation of a cellular network 16
  - Triangulation procedure 16
  - Effective number of triangles 16
- 3. Triangle shape 17
  - Side vectors of the reference triangle 17
  - Extraction of shape properties from the triangle shape transformation tensor 17
  - Geometrical interpretation of the triangle elongation tensor 17
- 4. Relation between triangle shape and triangle deformation 18
  - Pure shear by triangle elongation change 18
  - Shear-induced triangle rotation 18
- 5. Large-scale pure shear 19
  - Relation to average elongation 19
  - Alternative definition for the mean-field corotational term 19
  - Correlation terms arising from convective and corotational terms 19
- 6. Pure shear by a single T1 transition 20
  - Special case: square or rhombus 21

* mmerkel@syr.edu
† julicher@pks.mpg.de

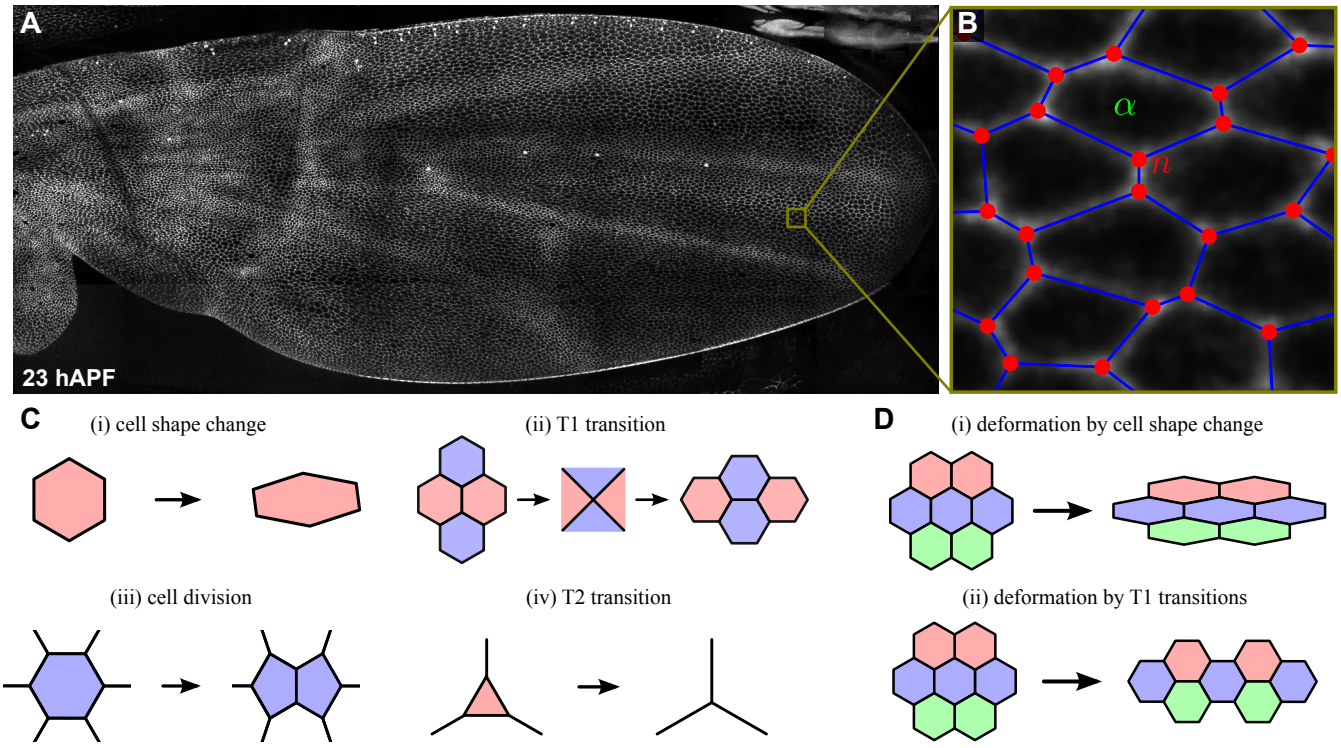

FIG. 1. (A) The developing fly wing is an important model system to study epithelial morphogenesis. This panel shows the wing blade at the developmental time of 23 hours after puparium formation (hAPF). (B) Magnified region of membrane-stained wing tissue overlaid with the corresponding polygonal network. Cells are represented by polygons (green), cell-cell interfaces correspond to polygon edges (blue), and polygon corners correspond to vertices (red). (C) We consider four kinds of cell-scale processes. (D) Two examples for pure shear of a piece of cellular material. (i) Pure shear by cell shape change. (ii) Pure shear by T1 transitions. Colors in panels C and D indicate cell identities.

7. Cellular contributions to isotropic expansion of a polygonal network 21
8. Cellular contributions to large-scale rotation in a triangle network 22
9. Path-dependence of the cumulative pure shear 23

B. Analysis of experimental data 23
1. Quantification of spatially averaged cellular deformation contributions 23
2. Spatial patterns of shear components 25
Infinitesimal time intervals 25
Finite time intervals 25

C. Comparison to related approaches 26

References 27

I. INTRODUCTION

Morphogenesis is the process in which a complex organism forms from a fertilized egg. Such morphogenesis involves the formation and dynamic reorganization of tissues [1–6]. An important type of tissues are epithelia, which are composed of two-dimensional layers of cells. During development, epithelia can undergo large-scale remodeling and deformations. This tissue dynamics can be driven by both internal and external stresses [3, 6]. Large-scale deformations are the result of many individual cellular processes such as cellular shape changes, cell divisions, cell rearrangements, and cell extrusions. The relationship between cellular processes and large-scale tissue deformations is key for an understanding of morphogenetic processes. In this paper, we provide a theoretical framework that can exactly relate cellular events to large-scale tissue deformations.

Modern microscopy techniques provide live image data of the development of animal tissues *in vivo* [3–8]. An important example is the fly wing, where about 10^4 cells have been tracked over 17 hours (Fig. 1A) [6]. Using cell membrane markers, semi-automated image analysis can segment the geometrical outlines and the neighbor relationships of all observed cells, and track their lineage throughout the process (Fig. 1B) [3, 8–12]. This provides detailed information about many different cellular events such as cell shape changes, cell rearrangements, cell division, and cell extrusions.

As a result of a large number of such cellular events, the cellular network is remodeled and undergoes changes in shape. Such shape changes can be described as tissue deformations using concepts from continuum mechan-

ics. The aim of this paper is to provide a framework to describe the geometry of tissue remodeling at different scales. We identify the contributions to tissue deformation stemming from cell shape changes and from distinct cellular processes that remodel the cellular network (Fig. 1C). For example, tissue shear can result from shape changes of individual cells or alternatively from cell rearrangements without cells changing their shape (Fig. 1D). In general, tissue deformations involve a combination of such events. Furthermore, cell divisions and extrusions also contribute to tissue deformations.

The relationship between tissue deformations and cellular events have been discussed in previous work [13–18]. Here, in order to obtain an exact decomposition of tissue deformation, we present a Triangle Method that is based on the dual network to the polygonal cellular network. We have recently presented a quantitative study of the *Drosophila* pupal wing morphogenesis using this approach [6].

In the following sections Sections II-V, we provide the mathematical foundations of the Triangle Method to characterize tissue remodeling. In Section II, we introduce a polygonal network description of epithelial cell packings. We discuss different types of topological changes of the network that are associated with cellular rearrangements and we define the deformation fields of the network. In Section III, we define mathematical objects that characterize triangle geometry and derive the relation between triangle shape changes and network deformations. Section IV presents the contribution of individual topological changes to network deformations. Section V combines the concepts developed in the preceding sections. We discuss the decomposition of large-scale tissue deformation into contributions resulting from large numbers of individual cellular processes. In Section VI, we apply the Triangle Method to the developing fly wing, comparing morphogenetic processes in different subsections of the wing blade. Finally, we discuss our results in Section VII. Technical details are provided in the Appendices A 1–B 2, while Appendix C compares our work to related approaches.

II. POLYGONAL AND TRIANGULAR NETWORKS

We introduce quantities to characterize small-scale and large-scale material deformation. To this end, we first discuss two complementary descriptions of epithelial cell packing geometry.

A. Description of epithelia as a network of polygons

The cell packing geometry of a flat epithelium can be described by a network of polygons, where each cell is represented by a polygon and each cell-cell interface corresponds to a polygon edge (Fig. 1B, Fig. 2A) [19]. Polygon corners are referred to as vertices, and a vertex belonging to M polygons is denoted M-fold vertex. Thus, the polygonal network captures the topology and geometry of the junctional network of the epithelium.

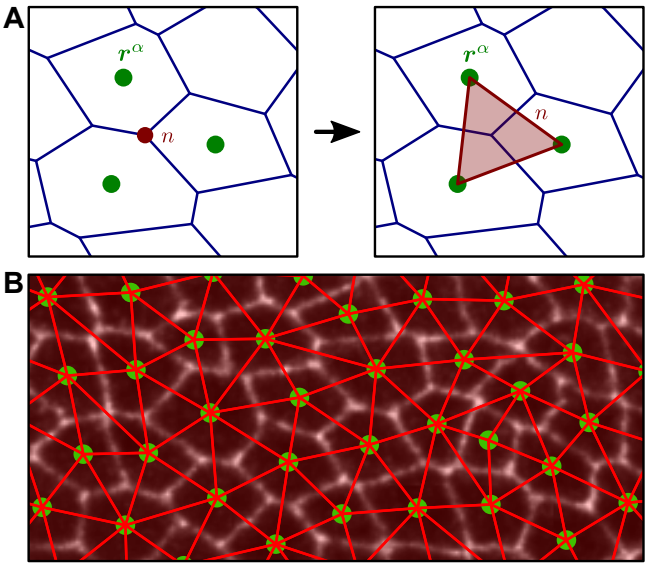

FIG. 2. Triangulation of the cellular network. (A) Each threefold vertex n (red dot) gives rise to a single triangle (red), which is also denoted by n. The corners of the triangle are defined by the centers of the three abutting cells (green dots). (B) Triangulation (red) on top of membrane-stained biological tissue (white). There are no gaps between the triangles.

Within such a polygonal network, we consider four kinds of cellular processes (Fig. 1C). (i) Polygons may change their shapes due to movement of vertices. (ii) Polygons may rearrange by changing their neighbors. A T1 transition is an elementary neighbor exchange during which two cells (red) lose their common edge, and two other cells (blue) gain a common edge. However, a T1 transition could also just occur partially. For instance, a single edge can shrink to length zero giving rise to an M-fold vertex with $M > 3$. Conversely, an M-fold vertex with $M > 3$ can split into two vertices that are connected by an edge. (iii) A polygon may split into two by cell division. (iv) A T2 transition corresponds to the extrusion of a cell from the network such that the corresponding polygon shrinks to a vertex. Note that the first process corresponds to a purely geometrical deformation whereas the last three processes correspond to topological transitions in the cellular network.

B. Triangulation of a polygonal network

To define contributions of cellular processes to the large-scale deformation of a polygonal network, we introduce a triangulation of the polygonal network (Fig. 2A). For each vertex n (red) being surrounded by three cells,

TABLE I. Notation used throughout this article.

Examples	
α, β, γ	Cell indices
n, m	Vertex and triangle indices
i, j, k	Dimension indices (either x or y)
$\boldsymbol{r}, \boldsymbol{h}$ and r_i, h_i	Vectors
$\mathbf{U}, \mathbf{s}^n$ and $\mathsf{U}_{ij}, \mathsf{s}^n_{ij}$	Tensors
$\tilde{\mathbf{U}}, \tilde{\mathbf{q}}^n$ and $\tilde{\mathsf{U}}_{ij}, \tilde{\mathsf{q}}^n_{ij}$	Symmetric, traceless tensors
$A, \tilde{\mathsf{Q}}_{ij}, \mathsf{U}_{ij}$	Large-scale quantities
$a^n, \tilde{\mathsf{q}}^n_{ij}, \mathsf{u}^n_{ij}$	Triangle-related quantities
$\Delta A, \Delta\tilde{\mathsf{Q}}_{ij}$	Finite quantities
$\delta A, \delta\mathsf{U}_{ij}$	Infinitesimal quantities

a triangle n (red) is created by defining its corners to coincide with the centers $\boldsymbol{r}^\alpha$ of the three cells (green). For the special case of an M-fold vertex with $M > 3$, we introduce M triangles as described in Appendix A 2. The center of a given cell α is defined by the vector

$$\boldsymbol{r}^\alpha = \frac{1}{a^\alpha}\int_{a^\alpha} \boldsymbol{r}\,\mathrm{d}A, \tag{1}$$

where the integration is over the cell area a^α and $\boldsymbol{r}$ is a position vector (Table I). Since triangle corners correspond to cell centers, oriented triangle sides are referred to by a pair of cell indices $\langle\alpha\beta\rangle$, and the corresponding triangle side vector is given by

$$\boldsymbol{r}^{\langle\alpha\beta\rangle} = \boldsymbol{r}^\beta - \boldsymbol{r}^\alpha. \tag{2}$$

The so-created triangulation of the cellular material contains no gaps between the triangles. It can be regarded as the dual of the polygonal network (Fig. 2B).

C. The deformation tensor

To characterize the deformation of the cellular network, we define a deformation tensor U_{ij} that corresponds to the coarse-grained displacement gradient:

$$\mathsf{U}_{ij} = \frac{1}{A}\int \partial_i h_j\,\mathrm{d}A. \tag{3}$$

Here, A is the area of the coarse-graining region. The vector field $\boldsymbol{h}(\boldsymbol{r})$ describes the continuous displacement field with respect to the reference position $\boldsymbol{r}$, and the indices i, j denote the axes x, y of a Cartesian coordinate system. The region may in general encompass several cells or just parts of a single cell.

The deformation tensor U_{ij} can be expressed in terms of the displacements $\boldsymbol{h}(\boldsymbol{r})$ along the margin of the region (see Appendix A 1):

$$\mathsf{U}_{ij} = \frac{1}{A}\oint h_j\nu_i\,\mathrm{d}\ell. \tag{4}$$

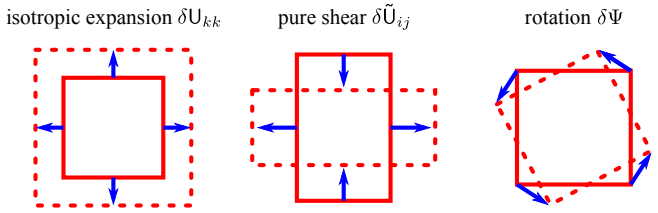

FIG. 3. Infinitesimal displacement gradients $\delta\mathsf{U}_{ij}$ can be decomposed into trace $\delta\mathsf{U}_{kk}$ describing isotropic expansion, symmetric, traceless part $\delta\tilde{\mathsf{U}}_{ij}$ describing pure shear, and antisymmetric part $\delta\Psi$ describing rotation.

Here, the vector $\boldsymbol{\nu}$ denotes the local unit vector that is normal to the margin pointing outwards.

For the case of infinitesimal deformations gradients $\delta\mathsf{U}_{ij} = \mathsf{U}_{ij}$, we decompose $\delta\mathsf{U}_{ij}$ into its trace $\delta\mathsf{U}_{kk}$ characterizing isotropic expansion, its symmetric, traceless part $\delta\tilde{\mathsf{U}}_{ij}$ characterizing pure shear, and its anisotropic part $\delta\Psi$ characterizing rotations (Fig. 3):

$$\delta\mathsf{U}_{ij} = \frac{1}{2}\delta\mathsf{U}_{kk}\delta_{ij} + \delta\tilde{\mathsf{U}}_{ij} - \delta\Psi\epsilon_{ij}. \tag{5}$$

Here, δ_{ij} denotes the Kronecker symbol and ϵ_{ij} is the generator of counter-clockwise rotations with $\epsilon_{xy} = -1$, $\epsilon_{yx} = 1$ and $\epsilon_{xx} = \epsilon_{yy} = 0$. Note that we mark symmetric, traceless tensors with a tilde and that we denote infinitesimal quantities by prepending a δ (Table I).

Eqs. (3) and (4) define the deformation tensor U_{ij} based on the continuous displacement field $\boldsymbol{h}(\boldsymbol{r})$. However for typical experiments, the displacement $\boldsymbol{h}(\boldsymbol{r})$ is only known for a finite number of positions $\boldsymbol{r}$. In the following, we will thus focus on the displacements of cell center positions $\boldsymbol{h}(\boldsymbol{r}^\alpha) = \boldsymbol{h}^\alpha$ and interpolate between them in order to compute the deformation tensor U_{ij}.

D. Triangle-based characterization of network deformation

We relate the large-scale deformation characterized by U_{ij} to small-scale deformation, which we quantify on the single-triangle level. We describe the deformation of a single triangle n from an initial to a final state by an affine transformation, which is characterized by a transformation tensor m^n_{ij} that maps each initial triangle side vector $\boldsymbol{r}^{\langle\alpha\beta\rangle}$ to the corresponding final side vector $\boldsymbol{r}'^{\langle\alpha\beta\rangle}$ (Fig. 4A):

$$r_i'^{\langle\alpha\beta\rangle} = \mathsf{m}^n_{ij} r_j^{\langle\alpha\beta\rangle}. \tag{6}$$

Note that Eq. (6) uniquely defines the tensor m^n_{ij}, which always exists [20]. However for polygons with more than three sides, no such tensor m^n_{ij} exists in general. This is the deeper reason for us to choose a triangle-based approach.

To relate triangle deformation to large-scale deformation U_{ij}, we first define a continuous displacement field

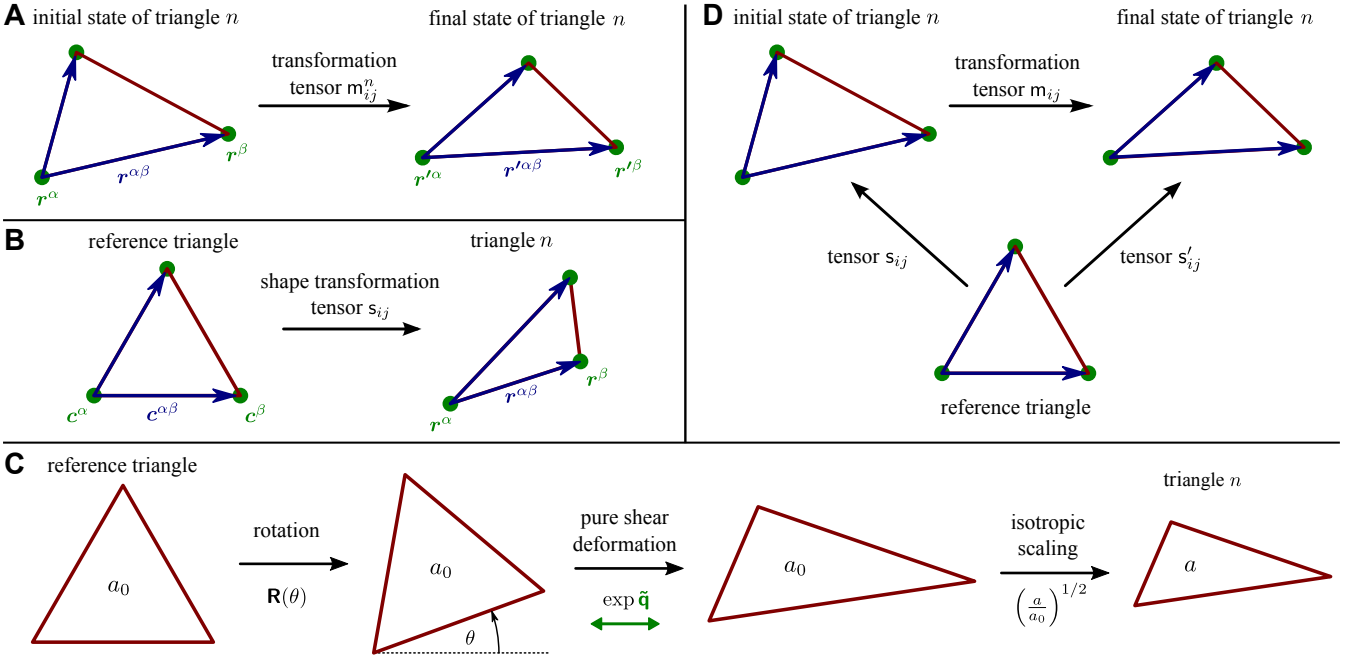

FIG. 4. Characterization of triangle deformation and shape. (A) Deformation of a triangle n from an initial state to a final state. The deformation is characterized by the linear transformation tensor m^n_{ij} mapping the initial sides vectors of the triangle to the final side vectors (blue arrows). (B) The shape of a triangle n in a given state is characterized by the tensor s_{ij}. Tensor s_{ij} maps the side vectors of a virtual equilateral reference triangle to the side vectors of triangle n (blue arrows). (C) Shape properties of a triangle n. The transformation tensor s_{ij} is decomposed into a counter-clockwise rotation by the triangle orientation angle θ, a pure shear deformation characterized by the triangle elongation tensor $\tilde{\mathsf{q}}_{ij}$, and an isotropic rescaling to match the actual triangle area a. (D) Connection between triangle shape and triangle deformation. A triangle deforms from an initial state to a final state. Deformation, initial state, and final state are characterized by the tensors m_{ij}, s_{ij}, and s'_{ij}, respectively.

$\boldsymbol{h}(\boldsymbol{r})$ by linearly interpolating between cell center displacements $\boldsymbol{h}^\alpha$. For any position $\boldsymbol{r}$ that lies within a given triangle n, we define:

$$h_j(\boldsymbol{r}) = h_j^\alpha + (r_i - r_i^\alpha)\mathsf{u}^n_{ij}. \tag{7}$$

Here, α denotes one of the cells belonging to triangle n. Note that the value of $\boldsymbol{h}(\boldsymbol{r})$ does not depend on the choice of α [21]. The triangle deformation tensor u^n_{ij} is defined by

$$\mathsf{u}^n_{ij} = \mathsf{m}^n_{ji} - \delta_{ij}. \tag{8}$$

Note the exchanged order of indices at the transformation tensor m^n_{ji}. Eq. (7) defines the displacement field $\boldsymbol{h}(\boldsymbol{r})$ throughout the entire triangular network such that the displacement gradient is constant on the area of each triangle n, taking the value of the triangle deformation tensor: $\partial_i h_j = \mathsf{u}^n_{ij}$.

Based on this displacement field, the large-scale deformation tensor U_{ij} as defined in Eq. (3) can be expressed as the average triangle deformation tensor defined in Eq. (8):

$$\mathsf{U}_{ij} = \langle \mathsf{u}_{ij} \rangle . \tag{9}$$

Here, the brackets denote an area-weighted average:

$$\langle \mathsf{u}_{ij} \rangle = \frac{1}{A}\sum_n a^n \mathsf{u}^n_{ij} \tag{10}$$

with A being the sum of all triangle areas and a^n being the area of triangle n.

Using Eq. (4), the large-scale deformation tensor U_{ij} can also be computed from the displacements of cell centers along the margin of the triangular network. The margin is a chain of triangle sides, and carrying out the boundary integral in Eq. (4) for each triangle side, Eq. (9) can be exactly rewritten as:

$$\mathsf{U}_{ij} = \frac{1}{A}\sum_{\langle\alpha\beta\rangle} h_j^{\langle\alpha\beta\rangle}\nu_i^{\langle\alpha\beta\rangle}\Delta\ell^{\langle\alpha\beta\rangle}. \tag{11}$$

Here, $\langle\alpha\beta\rangle$ runs over all triangle sides along the boundary such that cell β succeeds cell α in clockwise order, and:

$$\nu_i^{\langle\alpha\beta\rangle}\Delta\ell^{\langle\alpha\beta\rangle} = \epsilon_{ik} r_k^{\langle\alpha\beta\rangle} \tag{12}$$

$$h_j^{\langle\alpha\beta\rangle} = \frac{1}{2}(h_j^\alpha + h_j^\beta). \tag{13}$$

Thus, the vector $\nu_i^{\langle\alpha\beta\rangle}$ is the unit vector normal to side $\langle\alpha\beta\rangle$, pointing outside, the scalar $\Delta\ell^{\langle\alpha\beta\rangle}$ is the length of

side $\langle\alpha\beta\rangle$, and the vector $h_j^{\langle\alpha\beta\rangle}$ is its average displacement.

III. TRIANGLE SHAPES AND NETWORK DEFORMATION

We examine the relationship between large-scale deformation and cellular shape changes. To this end, we introduce quantities characterizing the shape of single triangles, and discuss their precise relation to triangle deformation.

A. Shape and orientation of a single triangle

Here, we define a symmetric, traceless tensor $\tilde{\mathsf{q}}_{ij}^n$ and an angle θ^n that together uniquely characterize the shape of a triangle n. We call $\tilde{\mathsf{q}}_{ij}^n$ the *triangle elongation*, which is a state variable that specifies the shape anisotropy of a given triangle. For simplicity, we omit the subscript n when discussing a single triangle.

We start by introducing a shape transformation tensor s_{ij}, which generates a given triangle n from an equilateral reference triangle (Fig. 4B). More precisely, each side vector $\boldsymbol{c}^{\langle\alpha\beta\rangle}$ of the equilateral reference triangle is mapped to the corresponding side vector $\boldsymbol{r}^{\langle\alpha\beta\rangle}$ of the given triangle n:

$$r_i^{\langle\alpha\beta\rangle} = \mathsf{s}_{ij} c_j^{\langle\alpha\beta\rangle}. \tag{14}$$

We choose the reference triangle to have area a_0 and one side aligned with the x axis. Its side vectors $\boldsymbol{c}^{\langle\alpha\beta\rangle}$ are defined in Appendix A 3. Note that Eq. (14) uniquely defines the shape transformation tensor s_{ij}.

The elongation tensor $\tilde{\mathsf{q}}_{ij}$ can be extracted from the shape transformation tensor s_{ij} by expressing s_{ij} as the tensor product of a rotation by the triangle orientation angle θ, a pure shear transformation parametrized by the elongation tensor $\tilde{\mathsf{q}}_{ij}$, and an area scaling (Fig. 4C):

$$\mathbf{s} = \left(\frac{a}{a_0}\right)^{1/2} \exp\left(\tilde{\mathbf{q}}\right) \cdot \mathbf{R}(\theta). \tag{15}$$

Here, we denote tensors by bold symbols. The exponential of a tensor is defined by the Taylor series of the exponential function, the dot denotes the tensor product, and the tensor $\mathbf{R}(\theta) = \exp(\theta\boldsymbol{\epsilon})$ denotes a counter-clockwise rotation by θ. Note that the exponential of a symmetric, traceless tensor has determinant one and describes a pure shear transformation. Also note that for given s_{ij}, Eq. (15) uniquely defines triangle area a, triangle elongation $\tilde{\mathsf{q}}_{ij}$, and the absolute triangle orientation angle θ (see Appendix A 3, [22], [23]).

Norm and axis of the elongation tensor

$$\tilde{\mathbf{q}} = |\tilde{\mathsf{q}}| \begin{pmatrix} \cos(2\phi) & \sin(2\phi) \\ \sin(2\phi) & -\cos(2\phi) \end{pmatrix} \tag{16}$$

are given by $|\tilde{\mathsf{q}}| = [(\tilde{\mathsf{q}}_{xx})^2 + (\tilde{\mathsf{q}}_{xy})^2]^{1/2} = [\mathrm{Tr}\,(\tilde{\mathbf{q}}^2)/2]^{1/2}$ and the angle ϕ (see Appendix A 3).

Note that the pure shear transformation $\exp(\tilde{\mathbf{q}})$ and the rotation $\mathbf{R}(\theta)$ in Eq. (15) do not commute. Exchanging both in Eq. (15) leads to a different definition of the elongation angle $\phi \mapsto \phi - \theta$, whereas the elongation norm $|\tilde{\mathsf{q}}|$ and the triangle orientation angle θ remain unchanged.

B. Triangle deformations corresponding to triangle shape changes

To reveal the precise relationship between triangle deformation and triangle shape, we consider again the deformation of a triangle n, which is characterized by the tensor m_{ij} (Fig. 4D). We denote the initial and final shape transformation tensors of the triangle by s_{ij} and s'_{ij}, respectively. Since both shape transformation tensors are defined with respect to the same reference triangle, the following relation holds:

$$\mathsf{s}'_{ij} = \mathsf{m}_{ik}\,\mathsf{s}_{kj}. \tag{17}$$

Based on this equation, the triangle deformation tensor u_{ij} can be expressed in terms of triangle shape change. For infinitesimal triangle deformations $\delta\mathsf{u}_{ij} = \mathsf{u}_{ij}$, trace $\delta\mathsf{u}_{kk}$, symmetric, traceless part $\delta\tilde{\mathsf{u}}_{ij}$, and antisymmetric part $\delta\psi$ describe isotropic expansion, pure shear and rotation as in Eq. (5):

$$\delta\mathsf{u}_{ij} = \frac{1}{2}\delta\mathsf{u}_{kk}\delta_{ij} + \delta\tilde{\mathsf{u}}_{ij} - \delta\psi\epsilon_{ij}. \tag{18}$$

These deformation components can be computed from the corresponding infinitesimal changes $\delta\tilde{\mathsf{q}}_{ij}$, δa, $\delta\theta$ of the triangle shape properties $\tilde{\mathsf{q}}_{ij}$, a, θ (see Appendix A 4):

$$\delta\tilde{\mathsf{u}}_{ij} = \delta\tilde{\mathsf{q}}_{ij} + \delta\tilde{\mathsf{j}}_{ij} \tag{19}$$

$$\delta\mathsf{u}_{kk} = \delta(\ln a) \tag{20}$$

$$\delta\psi = \delta\phi + (\delta\theta - \delta\phi)\cosh(2|\tilde{\mathsf{q}}|) \tag{21}$$

with

$$\delta\tilde{\mathsf{j}}_{ij} = -2\Big[g\delta\theta + (1-g)\delta\phi\Big]\epsilon_{ik}\tilde{\mathsf{q}}_{kj}. \tag{22}$$

Here, we have set $g = \sinh(2|\tilde{\mathsf{q}}|)/2|\tilde{\mathsf{q}}|$ and $\delta\phi$ denotes the change of the elongation axis angle ϕ. Eqs. (19)–(21) have interesting geometric interpretations for time-continuous shape changes.

For example Eq. (19), which relates triangle shear to triangle elongation, can be considered for an infinitesimal time interval δt. The pure shear rate $\tilde{\mathsf{v}}_{ij}$ of a triangle then obeys $\tilde{\mathsf{v}}_{ij}\delta t = \delta\tilde{\mathsf{u}}_{ij}$. According to Eq. (A20) in Appendix A 4, the pure shear rate corresponds exactly to a time derivative of $\tilde{\mathsf{q}}_{ij}$:

$$\tilde{\mathsf{v}}_{ij} = \frac{\mathrm{D}\tilde{\mathsf{q}}_{ij}}{\mathrm{D}t}. \tag{23}$$

This generalized corotational time derivative is defined by $(\mathrm{D}\tilde{\mathsf{q}}_{ij}/\mathrm{D}t)\delta t = \delta\tilde{\mathsf{q}}_{ij} + \delta\tilde{\mathsf{J}}_{ij}$, which can be rewritten as

$$\frac{\mathrm{D}\tilde{\mathsf{q}}_{ij}}{\mathrm{D}t} = \frac{\mathrm{d}\tilde{\mathsf{q}}_{ij}}{\mathrm{d}t} - 2\left(c\omega + (1-c)\frac{\mathrm{d}\phi}{\mathrm{d}t}\right)\epsilon_{ik}\tilde{\mathsf{q}}_{kj}. \tag{24}$$

Here, the operator $\mathrm{d}/\mathrm{d}t$ denotes the total time derivative of a quantity, $c = \tanh(2|\tilde{\mathsf{q}}|)/2|\tilde{\mathsf{q}}|$, and ω is the triangle vorticity with $\omega\delta t = \delta\psi$. In the limit $|\tilde{\mathsf{q}}| \ll 1$ for which $c \simeq 1$, the generalized corotational derivative becomes the conventional Jaumann derivative [24]:

$$\frac{\mathrm{D}\tilde{\mathsf{q}}_{ij}}{\mathrm{D}t} \simeq \frac{\mathrm{d}\tilde{\mathsf{q}}_{ij}}{\mathrm{d}t} + \omega_{ik}\tilde{\mathsf{q}}_{kj} + \omega_{jk}\tilde{\mathsf{q}}_{ki}, \tag{25}$$

where we introduced $\omega_{ij} = -\omega\epsilon_{ij} = (\mathsf{v}_{ij} - \mathsf{v}_{ji})/2$. The general case of finite $|\tilde{\mathsf{q}}|$ with $c \neq 1$ is discussed in more detail in Appendix A 4.

According to Eq. (20), the isotropic triangle expansion rate v_{kk} with $\mathsf{v}_{kk}\delta t = \delta\mathsf{u}_{kk}$ can be written as:

$$\mathsf{v}_{kk} = \frac{1}{a}\frac{\mathrm{d}a}{\mathrm{d}t}. \tag{26}$$

The isotropic triangle expansion rate thus corresponds to the relative change rate of the triangle area a.

Finally, Eq. (21) states that the change of the triangle orientation angle θ can be written as (see Eq. (A22) in Appendix A 4)

$$\frac{\mathrm{d}\theta}{\mathrm{d}t} = \omega + \tilde{\mathsf{v}}_{ij}\epsilon_{jk}\tilde{\mathsf{q}}_{ki}\frac{\cosh(2|\tilde{\mathsf{q}}|) - 1}{2|\tilde{\mathsf{q}}|\sinh(2|\tilde{\mathsf{q}}|)}. \tag{27}$$

Hence, the triangle orientation angle θ may not only change due to a vorticity ω in the flow field, but also due to local pure shear. This shear-induced triangle rotation appears whenever there is a component of the shear rate tensor $\tilde{\mathsf{v}}_{ij}$ that is neither parallel nor perpendicular to the triangle elongation axis. We discuss this effect of shear-induced rotation in more detail in Appendix A 4.

C. Large-scale deformation of a triangular network

To understand how triangle shape properties connect to large-scale deformation of a triangle network, we coarse-grain Eqs. (19)-(21). We focus on the case where the shape properties $\tilde{\mathsf{q}}^n_{ij}$, a^n, θ^n of all involved triangles n change only infinitesimally. The large-scale deformation tensor of the triangular network can be computed using Eq. (9): $\delta\mathsf{U}_{ij} = \langle\delta\mathsf{u}_{ij}\rangle$. Consequently, one obtains large-scale pure shear as $\delta\tilde{\mathsf{U}}_{ij} = \langle\delta\tilde{\mathsf{u}}_{ij}\rangle$, large-scale isotropic expansion as $\delta\mathsf{U}_{kk} = \langle\delta\mathsf{u}_{kk}\rangle$, and large-scale rotation as $\delta\Psi = \langle\delta\psi\rangle$. We now express large-scale pure shear and isotropic expansion in terms of triangle shape changes. We discuss large-scale rotation in Appendix A 8.

1. *Pure shear deformation on large scales*

To discuss large-scale pure shear deformation, we first introduce an average triangle elongation tensor:

$$\tilde{\mathsf{Q}}_{ij} = \langle\tilde{\mathsf{q}}_{ij}\rangle\,. \tag{28}$$

The average is computed using an area weighting as in Eq. (10).

The large-scale pure shear tensor $\delta\tilde{\mathsf{U}}_{ij}$ can be related to the change of the average triangle elongation $\delta\tilde{\mathsf{Q}}_{ij}$ by averaging Eq. (19) over all triangles in the triangulation (see Appendix A 5):

$$\delta\tilde{\mathsf{U}}_{ij} = \delta\tilde{\mathsf{Q}}_{ij} + \delta\tilde{\mathsf{J}}_{ij} + \delta\tilde{\mathsf{K}}_{ij}. \tag{29}$$

Here, in analogy to Eqs. (24) and (A20), we introduced the mean-field corotational term

$$\delta\tilde{\mathsf{J}}_{ij} = -2\Big[C\delta\Psi + (1-C)\delta\Phi\Big]\epsilon_{ik}\tilde{\mathsf{Q}}_{kj}, \tag{30}$$

where $C = \tanh(2|\tilde{\mathsf{Q}}|)/2|\tilde{\mathsf{Q}}|$, and $|\tilde{\mathsf{Q}}|$ and Φ denote norm and angle of the average elongation tensor $\tilde{\mathsf{Q}}_{ij}$, respectively. Note that different definitions for $\delta\tilde{\mathsf{J}}_{ij}$ are possible and an alternative to Eq. (30) is presented in Appendix A 5. Moreover, the contribution $\delta\tilde{\mathsf{K}}_{ij}$ newly appears due to the averaging. It is the sum of two correlations:

$$\delta\tilde{\mathsf{K}}_{ij} = -\Big(\langle\delta\mathsf{u}_{kk}\tilde{\mathsf{q}}_{ij}\rangle - \delta\mathsf{U}_{kk}\tilde{\mathsf{Q}}_{ij}\Big) + \Big(\langle\delta\tilde{\mathsf{j}}_{ij}\rangle - \delta\tilde{\mathsf{J}}_{ij}\Big). \tag{31}$$

We call the first term *growth correlation* and the second term *rotational correlation*.

Growth correlation is created by spatial fluctuations in isotropic triangle expansion $\delta\mathsf{u}^n_{kk}$. Fig. 5A illustrates this effect for a deformation where no large-scale pure shear appears $\delta\tilde{\mathsf{U}}_{ij} = 0$. Two triangles with different but constant triangle elongation tensors $\tilde{\mathsf{q}}^n_{ij}$ deform: One triangle expands isotropically and the other triangle shrinks isotropically. Because of the area-weighting in the averaging, the average elongation tensor $\tilde{\mathsf{Q}}_{ij}$ thus changes during this deformation. Therefore, although $\delta\tilde{\mathsf{U}}_{ij} = 0$ in Eq. (29), the average elongation changes by $\delta\tilde{\mathsf{Q}}_{ij} \neq 0$. This change in average elongation is exactly compensated for by the growth correlation term.

Rotational correlation can be created by spatial fluctuations of triangle rotation $\delta\psi^n$. We illustrate this in Fig. 5B, where the large-scale pure shear rate is again zero $\delta\tilde{\mathsf{U}}_{ij} = 0$. We consider two triangles with the same area but different elongation tensors $\tilde{\mathsf{q}}^n_{ij}$. Both triangles do not deform, but rotate in opposing directions by the same absolute angle $\delta\psi^n$. The large-scale corotational term is zero $\delta\tilde{\mathsf{J}}_{ij} = 0$, because there is no overall rotation $\delta\Psi = 0$. However, the corotational term for each individual triangle $\delta\tilde{\mathsf{j}}^n_{ij}$ is nonzero allowing for a change of triangle elongation in the absence of triangle shear. After all, the average elongation tensor $\tilde{\mathsf{Q}}_{ij}$ increases along

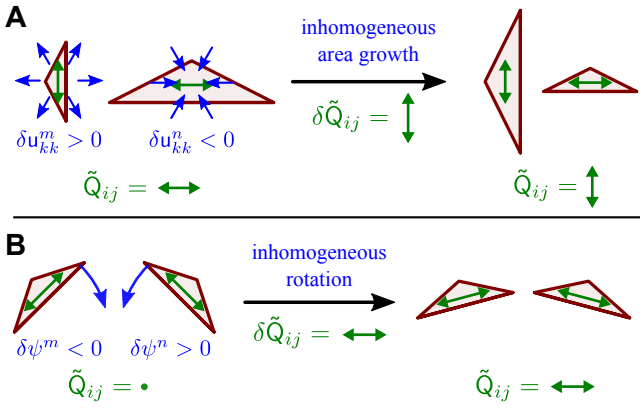

FIG. 5. Correlation contributions to pure shear. (A) Inhomogeneous isotropic expansion that is correlated with elongation creates a change in the average elongation $\tilde{\mathsf{Q}}_{ij}$, which is due to the area weighting in the definition of $\tilde{\mathsf{Q}}_{ij}$. This contribution to the time derivative of $\tilde{\mathsf{Q}}_{ij}$ is compensated for by the growth correlation term in $\delta\tilde{\mathsf{K}}_{ij}$. (B) Inhomogeneous rotation that is correlated with elongation creates a change in the average elongation $\tilde{\mathsf{Q}}_{ij}$. This contribution to the time derivative of $\tilde{\mathsf{Q}}_{ij}$ is compensated for by the rotational correlation term in $\delta\tilde{\mathsf{K}}_{ij}$.

the horizontal, because each individual triangle elongation tensor does. This change in average elongation is compensated for by the rotational correlation term.

To obtain the large-scale pure shear rate $\tilde{\mathsf{V}}_{ij}$ defined by $\tilde{\mathsf{V}}_{ij}\delta t = \delta\tilde{\mathsf{U}}_{ij}$, we rewrite Eq. (29):

$$\tilde{\mathsf{V}}_{ij} = \frac{\mathrm{D}\tilde{\mathsf{Q}}_{ij}}{\mathrm{D}t} + \tilde{\mathsf{D}}_{ij}. \tag{32}$$

Here, $\mathrm{D}\tilde{\mathsf{Q}}_{ij}/\mathrm{D}t$ denotes a corotational time derivative that is defined by $(\mathrm{D}\tilde{\mathsf{Q}}_{ij}/\mathrm{D}t)\delta t = \delta\tilde{\mathsf{Q}}_{ij} + \delta\tilde{\mathsf{J}}_{ij}$, which can be rewritten as

$$\frac{\mathrm{D}\tilde{\mathsf{Q}}_{ij}}{\mathrm{D}t} = \frac{\mathrm{d}\tilde{\mathsf{Q}}_{ij}}{\mathrm{d}t} - 2\left(C\Omega + (1-C)\frac{\mathrm{d}\Phi}{\mathrm{d}t}\right)\epsilon_{ik}\tilde{\mathsf{Q}}_{kj}. \tag{33}$$

Here, $C = \tanh(2|\tilde{\mathsf{Q}}|)/2|\tilde{\mathsf{Q}}|$ as defined below Eq. (30) and Ω is the average vorticity with $\omega\delta t = \delta\Psi$. The term $\tilde{\mathsf{D}}_{ij}$ in Eq. (32) contains the correlation terms with $\tilde{\mathsf{D}}_{ij}\delta t = \delta\tilde{\mathsf{K}}_{ij}$.

Eq. (32) is an important result for the case without topological transitions. It states that the large-scale deformation of a triangular network can be computed from the change of the average triangle elongation, the correlation between triangle elongation and triangle area growth, and the correlation between triangle elongation and triangle rotation.

The correlations account for the fact that taking the corotational derivative does not commute with averaging:

$$\tilde{\mathsf{D}}_{ij} = \left\langle \frac{\mathrm{D}\tilde{\mathsf{q}}_{ij}}{\mathrm{D}t} \right\rangle - \frac{\mathrm{D}\tilde{\mathsf{Q}}_{ij}}{\mathrm{D}t}. \tag{34}$$

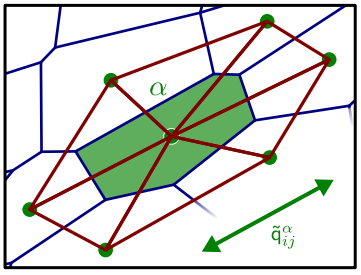

FIG. 6. The elongation $\tilde{\mathsf{q}}^{\alpha}_{ij}$ of a cell α (green) is defined by the average elongation of the triangles belonging to α (red). The triangles belonging to α are those that have one of their corners defined by the center of α.

In particular, as illustrated in Fig. 5B, the rotational correlation arises by coarse-graining of the corotational term. Similarly, the growth correlation can be regarded as arising from the coarse-graining of a convective term (see Appendix A 5).

2. *Elongation and shear of a single cell*

To more explicitly relate the above discussion to cell shape and deformation, we define a cell elongation tensor $\tilde{\mathsf{q}}^{\alpha}_{ij}$ for a given cell α as follows. We select all triangles n that have one of their corners defined by the center of α, and then average their elongation tensors (Fig. 6):

$$\tilde{\mathsf{q}}^{\alpha}_{ij} = \langle \tilde{\mathsf{q}}_{ij} \rangle . \tag{35}$$

The average is again area-weighted as defined in Eq. (10). Then, a cellular pure shear rate can be defined analogously: $\tilde{\mathsf{v}}^{\alpha}_{ij} = \langle \tilde{\mathsf{v}}_{ij} \rangle$. This cellular pure shear rate can also be expressed by changes of $\tilde{\mathsf{q}}^{\alpha}_{ij}$ using Eq. (32). Moreover, the large-scale elongation $\tilde{\mathsf{Q}}_{ij}$ and the large-scale pure shear rate $\tilde{\mathsf{V}}_{ij}$ can be obtained by suitably averaging the single-cell quantities $\tilde{\mathsf{q}}^{\alpha}_{ij}$ and $\tilde{\mathsf{v}}^{\alpha}_{ij}$ [25].

3. *Isotropic expansion on large scales*

Finally, we discuss large-scale isotropic expansion $\delta\mathsf{U}_{kk}$ of a triangle network. We relate it to changes of the average triangle area $\bar{a} = A/N$, where A is the total area of the network and N is the number of triangles in the network.

To relate large-scale isotropic expansion $\delta\mathsf{U}_{kk}$ to changes of the average triangle area $\bar{a}$, we average Eq. (20):

$$\delta\mathsf{U}_{kk} = \delta(\ln\bar{a}). \tag{36}$$

Accordingly, the large-scale isotropic expansion rate V_{kk} with $\mathsf{V}_{kk}\delta t = \delta\mathsf{U}_{kk}$ can be expressed as

$$\mathsf{V}_{kk} = \frac{1}{\bar{a}}\frac{\mathrm{d}\bar{a}}{\mathrm{d}t}. \tag{37}$$

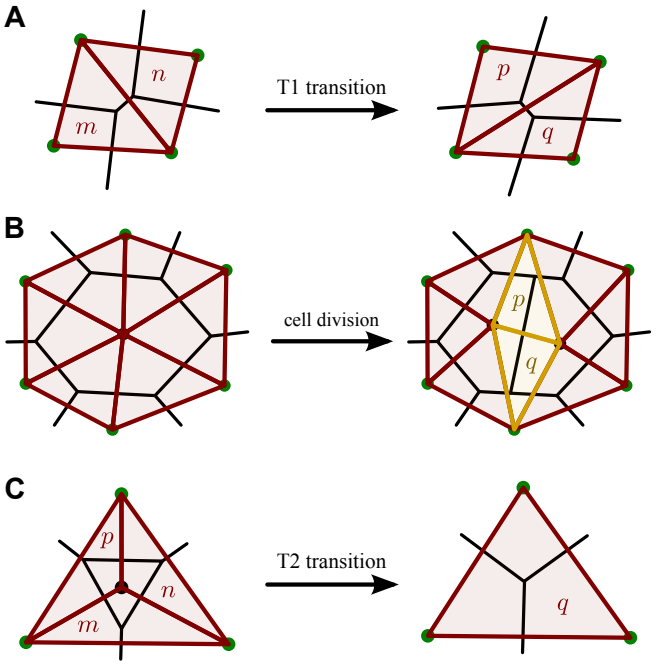

FIG. 7. Effects of a single topological transition on the triangulation. (A) A T1 transition removes two triangles (m and n) and creates two new ones (p and q). (B) A cell division creates two triangles (p and q, yellow). All other triangles shown (red) change their shape instantaneously. (C) A T2 transition removes three triangles (m, n, p) and creates a new one (q).

Hence, large-scale isotropic expansion corresponds to the relative change of the average triangle area $\bar{a}$.

IV. CONTRIBUTIONS OF TOPOLOGICAL TRANSITIONS TO NETWORK DEFORMATION

So far, we have considered deformations of a triangular network during which no topological transitions occur. Now, we discuss the contributions of topological transitions to large-scale deformations [26].

There are two main features of topological transitions that motivate the following discussion. First, topological transitions occur instantaneously at precise time points t_k and correspondingly, there is no displacement of cell centers upon topological transitions.

Second, topological transitions create and remove triangles from the triangulation. For instance for the typical case of three-fold vertices, a T1 transition removes two triangles and then adds two new triangles (Fig. 7A), a cell division just adds two triangles (Fig. 7B), and a T2 transitions removes three triangles and adds one new triangle (Fig. 7C).

To define the large-scale deformation tensor across a given topological transition, an average over triangle deformations as in Eq. (9) can no longer be used because the triangle deformation tensor u_{ij}^n is ill-defined for disappearing and appearing triangles. We thus define the large-scale deformation depending on cell center displacements along the margin of the triangular network using Eq. (11). We denote such a large-scale deformation tensor across a topological transition by $\Delta\mathsf{U}_{ij}$. Because there are no cell center displacements upon a topological transition, the large-scale deformation tensor vanishes $\Delta\mathsf{U}_{ij} = 0$, and so does large-scale isotropic expansion $\Delta\mathsf{U}_{kk} = 0$ and large-scale pure shear $\Delta\tilde{\mathsf{U}}_{ij} = 0$. However, even though there is no actual network deformation *upon* a topological transition, we will define the deformation contribution *by* a topological transition in the following.

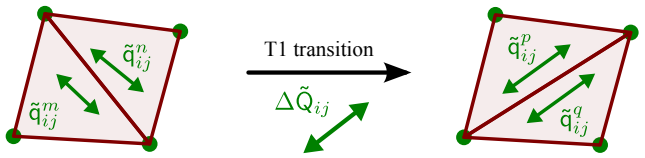

FIG. 8. A T1 transition induces an instantaneous change of the average triangle elongation. The average triangle elongation before and after the T1 transition only depends on the position of the four involved cell centers (green dots).

A. Contribution of a single topological transition to pure shear

To discuss the pure shear contribution by a topological transition, we focus on a single T1 transition occurring at time t_k. Pure shear contributions by cell divisions or T2 transitions can be discussed analogously.

Because of the triangulation change during a T1 transition, the average triangle elongation $\tilde{\mathsf{Q}}_{ij}$ changes instantaneously by a finite amount $\Delta\tilde{\mathsf{Q}}_{ij}$ (Fig. 8). To account for the shear contribution by the T1 transition, we introduce an additional term $\Delta\tilde{\mathsf{X}}_{ij}$ into the shear balance Eq. (29):

$$\Delta\tilde{\mathsf{U}}_{ij} = \Delta\tilde{\mathsf{Q}}_{ij} + \Delta\tilde{\mathsf{X}}_{ij}. \tag{38}$$

Here, we have set corotational and correlation terms during the T1 transition to zero [27]. Because $\Delta\tilde{\mathsf{U}}_{ij} = 0$, we obtain from Eq. (38) that $\Delta\tilde{\mathsf{X}}_{ij} = -\Delta\tilde{\mathsf{Q}}_{ij}$. Thus, the shear contribution $\Delta\tilde{\mathsf{X}}_{ij}$ due to the T1 transition compensates for the finite discontinuity in $\tilde{\mathsf{Q}}_{ij}$, which occurs due to the removal and addition of triangles.

Dividing by a time interval Δt and in the limit $\Delta t \to 0$, we can transform Eq. (38) into an equation for the shear rate:

$$\tilde{\mathsf{V}}_{ij} = \frac{\mathrm{D}\tilde{\mathsf{Q}}_{ij}}{\mathrm{D}t} + \tilde{\mathsf{D}}_{ij} + \tilde{\mathsf{T}}_{ij}, \tag{39}$$

where $\tilde{\mathsf{T}}_{ij} = \Delta\tilde{\mathsf{X}}_{ij}\delta(t - t_k)$ and δ denotes the Dirac delta function. Hence, a T1 transition induces a discontinuity in the average triangle elongation $\tilde{\mathsf{Q}}_{ij}$, causing a delta peak in $\mathrm{D}\tilde{\mathsf{Q}}_{ij}/\mathrm{D}t$. This delta peak is exactly compensated

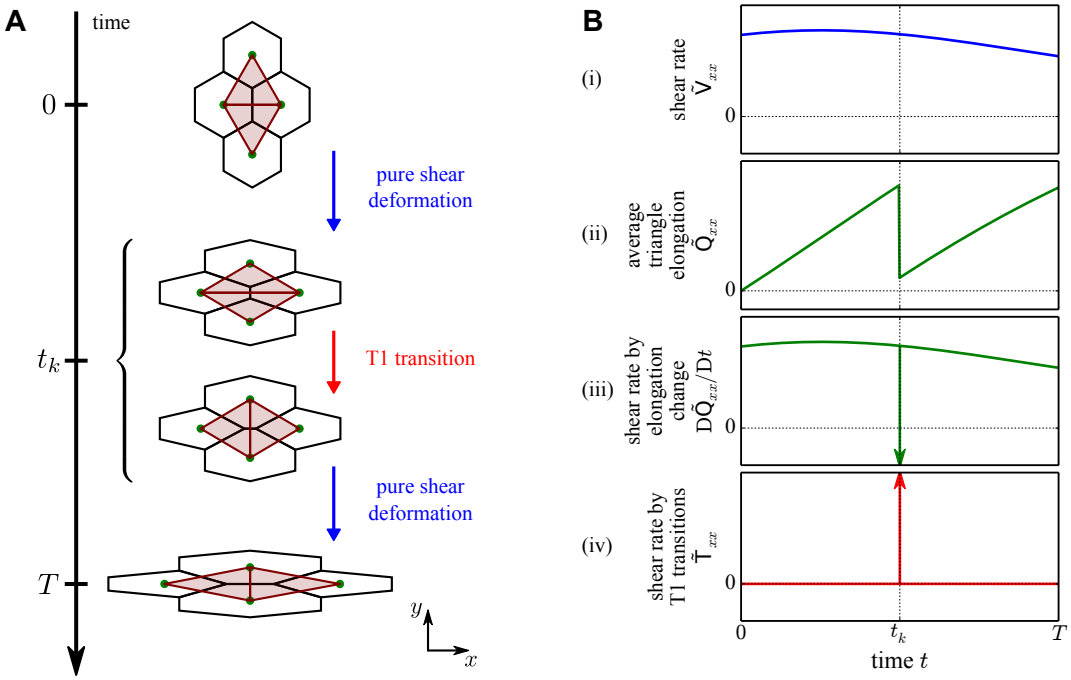

FIG. 9. Illustration of the shear rate contributions by average triangle elongation change and T1 transitions. (A) Between the time points 0 and T, a triangular network is continously sheared along the horizontal axis. At time point t_k, a T1 transition occurs, which instantaneously changes the average triangle elongation. (B) For the process shown in panel A, schematic time-dependent plots of shear rate (blue, i), the average triangle elongation (green, ii), its derivative (green, iii), and the shear rate by T1 transitions (red, iv). For each tensor, the respective xx component, i.e. the horizontal component, is plotted. The arrows in (iii) and (iv) indicate Dirac δ peaks. Their magnitude corresponds to the step in $\tilde{\mathsf{Q}}_{xx}$ at t_k.

for by $\Delta\tilde{\mathsf{X}}_{ij}\delta(t-t_k)$, such that the large-scale shear rate $\tilde{\mathsf{V}}_{ij}$ contains no delta peaks.

As an example, Fig. 9A illustrates a process during which a network consisting of two triangles (red) is being deformed between the times 0 and T. These triangles undergo a pure shear deformation along the x axis without any rotations or inhomogeneities. In the absence of any topological transition, the shear rate along the x axis, $\tilde{\mathsf{V}}_{xx}$, corresponds to the derivative of the average triangle elongation, $\mathrm{d}\tilde{\mathsf{Q}}_{xx}/\mathrm{d}t$ (Fig. 9B(i-iii)). However, at a time point t_k, a T1 transition occurs and the average elongation along the x axis changes instantaneously by $\Delta\tilde{\mathsf{Q}}_{xx}$. Thus, there is a Dirac δ peak in $\mathrm{d}\tilde{\mathsf{Q}}_{xx}/\mathrm{d}t$, which is compensated by the T1 shear rate $\tilde{\mathsf{T}}_{xx} = -\Delta\tilde{\mathsf{Q}}_{xx}\delta(t-t_k)$ (Fig. 9B(iv)) such that Eq. (39) holds exactly.

For the special case where the four cell centers involved in the T1 transition (green dots in Fig. 8) form a square, the magnitude of $\Delta\tilde{\mathsf{X}}_{ij}$ evaluates exactly to $|\Delta\tilde{\mathsf{X}}| = (A_\square \ln 3)/(2A)$, where $A_\square$ is the area of the square and A is the total area of the triangle network (see Appendix A 6). The axis of $\Delta\tilde{\mathsf{X}}_{ij}$ is along one of the diagonals of the square. Both remain true for the more general case of a rhombus, i.e. a quadrilateral whose four sides have equal lengths.

B. Contribution of a single topological transition to isotropic expansion

To define the isotropic expansion by a topological transition, we employ a similar argument as for the pure shear component. For instance, to account for the isotropic expansion by a single cell division occurring at time t_k, we introduce a term Δd into Eq. (36) (cell extrusions can be treated analogously):

$$\Delta\mathsf{U}_{kk} = \Delta(\ln\bar{a}) + \Delta d. \tag{40}$$

Here, $\Delta(\ln\bar{a})$ denotes the change of $\ln\bar{a}$ across the cell division. Since there is no isotropic expansion upon the cell division $\Delta\mathsf{U}_{kk} = 0$, we thus have $\Delta d = -\Delta(\ln\bar{a})$. Because the total area A of the triangulation remains constant during the cell division, the isotropic expansion by a cell division amounts to $\Delta d = \ln(1+2/N)$ with N being the number of triangles in the network before the division.

Dividing by a time interval Δt and in the limit $\Delta t \to 0$, Eq. (40) transforms into:

$$\mathsf{V}_{kk} = \frac{\mathrm{d}(\ln\bar{a})}{\mathrm{d}t} + k_d \tag{41}$$

with $k_d = \ln(1+2/N)\,\delta(t-t_k)$. Hence, as for the pure shear component, the contributions of individual topo-

logical transitions to the isotropic expansion component can be accounted for by delta peaks.

Note that in order to avoid isotropic expansion contributions by T1 transitions, care has to be taken when counting the number of triangles N for the special case of M-fold vertices with $M > 3$. In Appendix A 2, we explain how we define N in this case.

V. CELLULAR CONTRIBUTIONS TO THE LARGE-SCALE DEFORMATION RATE

In this section, we provide equations that express large-scale pure shear and isotropic expansion as sums of all cellular contributions. Large-scale rotation is discussed in Appendix A 8. Here, we present the equations for the deformation rates, i.e. in the limit of infinitesimal deformations. The case of finite deformations is discussed in Appendix B.

A. Pure shear rate

We decompose the instantaneous large-scale shear rate $\tilde{\mathsf{V}}_{ij}$ into the following cellular contributions:

$$\tilde{\mathsf{V}}_{ij} = \frac{\mathrm{D}\tilde{\mathsf{Q}}_{ij}}{\mathrm{D}t} + \tilde{\mathsf{T}}_{ij} + \tilde{\mathsf{C}}_{ij} + \tilde{\mathsf{E}}_{ij} + \tilde{\mathsf{D}}_{ij}. \tag{42}$$

The first term on the right-hand side denotes the corotational time derivative of $\tilde{\mathsf{Q}}_{ij}$ defined by Eq. (33). Note that some care has to be taken when evaluating the corotational term in the presence of topological transitions (see Appendix A 6). The shear rate contributions by T1 transitions $\tilde{\mathsf{T}}_{ij}$, cell divisions $\tilde{\mathsf{C}}_{ij}$, and T2 transitions $\tilde{\mathsf{E}}_{ij}$ to the large-scale shear rate are respectively defined by

$$\tilde{\mathsf{T}}_{ij} = -\sum_{k\in\mathrm{T1}} \Delta\tilde{\mathsf{Q}}^k_{ij}\delta(t-t_k) \tag{43}$$

$$\tilde{\mathsf{C}}_{ij} = -\sum_{k\in\mathrm{CD}} \Delta\tilde{\mathsf{Q}}^k_{ij}\delta(t-t_k) \tag{44}$$

$$\tilde{\mathsf{E}}_{ij} = -\sum_{k\in\mathrm{T2}} \Delta\tilde{\mathsf{Q}}^k_{ij}\delta(t-t_k). \tag{45}$$

Here, the sums run over all topological transitions k of the respective kind, t_k denotes the time point of the respective transition, and $\Delta\tilde{\mathsf{Q}}^k_{ij}$ denotes the instantaneous change in $\tilde{\mathsf{Q}}_{ij}$ induced by the transition. Finally, $\tilde{\mathsf{D}}_{ij}$ denotes the shear rate by the correlation effects as introduced in Section III C 1.

B. Isotropic expansion rate

We decompose the isotropic expansion rate V_{kk} as follows into cellular contributions:

$$\mathsf{V}_{kk} = \frac{\mathrm{d}(\ln\bar{a})}{\mathrm{d}t} + k_d - k_e. \tag{46}$$

Here, $\bar{a}$ is the average triangle area as in Section III C 3, and k_d and k_e denote cell division and cell extrusion rates, defined as

$$k_d = \sum_{k\in\mathrm{CD}} \delta(t-t_k)\ln\left(1+\frac{2}{N_k}\right) \tag{47}$$

$$k_e = -\sum_{k\in\mathrm{T2}} \delta(t-t_k)\ln\left(1-\frac{2}{N_k}\right). \tag{48}$$

The sums run over all topological transitions k of the respective kind, t_k denotes the time point of the respective transition, and N_k is the number of triangles in the network before the respective transition.

Instead of formulating Eq. (46) for a triangulation, the polygonal network may also be used to derive such an equation. With the isotropic expansion rate for the polygonal network V^p_{kk}, the average cell area $\bar{a}^p$ and the topological contributions by divisions k^p_d and extrusions k^p_e, we obtain (see Appendix A 7):

$$\mathsf{V}^p_{kk} = \frac{\mathrm{d}(\ln\bar{a}^p)}{\mathrm{d}t} + k^p_d - k^p_e. \tag{49}$$

This equation can be interpreted as a continuum equation for cell density [28, 29], where the isotropic expansion rate contributions by cell divisions k^p_d and cell extrusions k^p_e correspond to cell division and cell extrusion rates, respectively.

C. Cumulative shear and expansion

Often, it is useful to consider cumulative deformations rather than deformation rates. The cumulative shear deformation is defined as $\int_{t_0}^{t_1}\tilde{\mathsf{V}}_{ij}\mathrm{d}t$, other cumulative quantities are defined correspondingly. Note that this cumulative shear deformation is not a deformation that only depends on the initial and final configurations at times t_0 and t_1, but it also depends on the full path the system takes between those two configurations (see Appendix A 9). The cumulative isotropic expansion $\int_{t_0}^{t_1}\mathsf{V}_{kk}\mathrm{d}t = \log A(t_1) - \log A(t_0)$ is independent of the full path and given by a change of tissue area between initial and final states. This follows from Eq. (37). The cumulative shear can be decomposed into cellular contributions. This decomposition can be obtained by integrating the decomposition of shear rates Eq. (42) over time. Similarly, the cumulative isotropic expansion can be decomposed into cellular contributions by integrating Eq. (46) over time.

VI. TISSUE REMODELING IN THE PUPAL FLY WING AS AN EXAMPLE

Our Triangle Method can be used to analyze tissue remodeling in the pupal fly wing [3, 6]. Here, we provide a

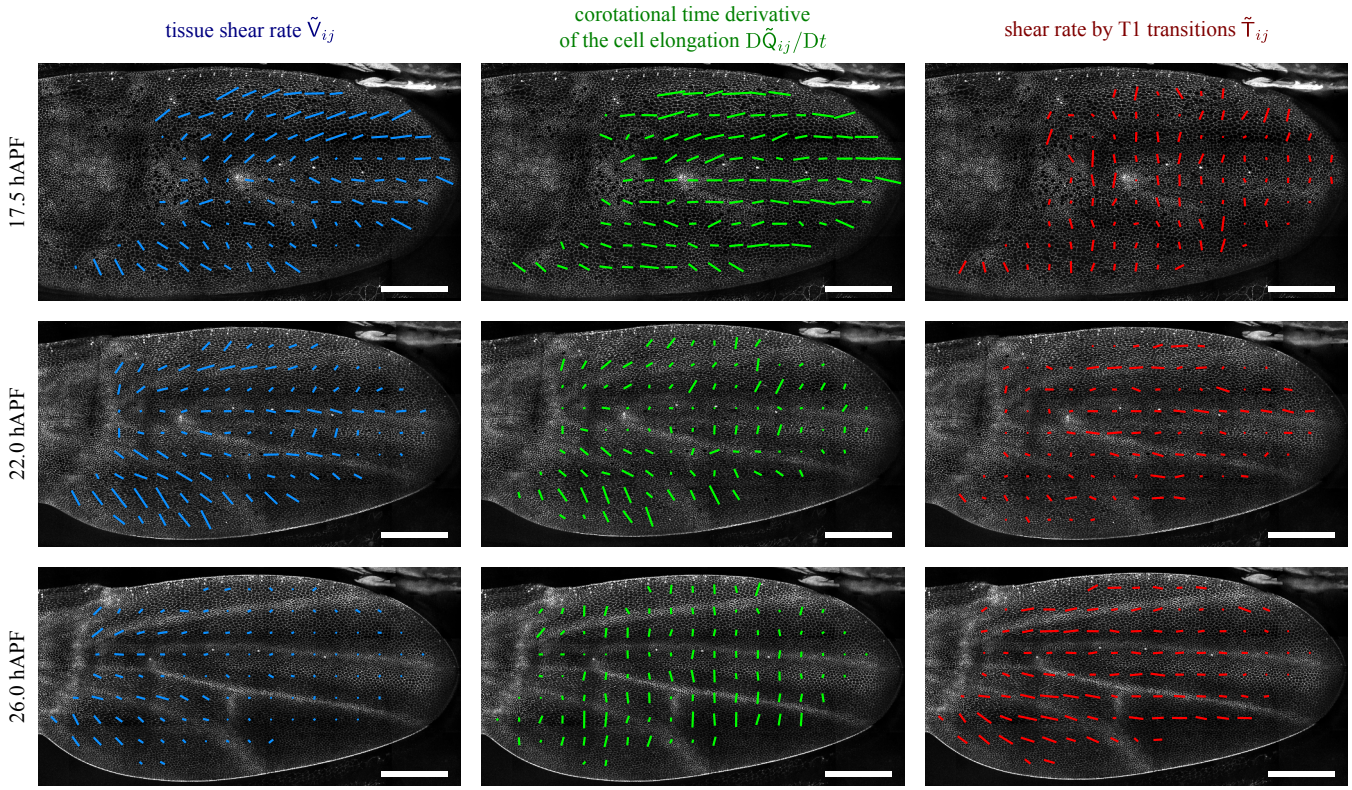

FIG. 10. Patterns of tissue shear and contributions to shear in the pupal wing of the fruit fly at different times in hours after puparium formation (hAPF). Local rate of pure shear (blue), corotational time derivative of the cell elongation (center), and shear rate by T1 transitions (right). The bars indicate the axis and norm of the tensors. Shown are averages over squares with size $(33\,\mu\mathrm{m})^2$ and over time intervals of about 2 h. The scale bars correspond to 100 µm.

more refined and in depth analysis of the wing morphogenesis data for three different wild type wings presented previously [6]. Differences to the previous analyses are (i) there are slightly improved definitions of the shear rates for finite time intervals between frames (see Appendix B 1) (ii) we now analyze and compare subregions of the wing tissue, which provides additional information about tissue remodeling.

Note that we have so far only discussed the case of infinitesimal deformations. However, the sampling rate of experimental data is necessarily finite. We explain how we treat such finite deformation data in detail in Appendix B.

Fig. 10 presents coarse-grained spatial patterns of local tissue shear $\tilde{\mathrm{V}}_{ij}$ (blue, left column), the corotational time derivative of the cell elongation $\mathrm{D}\tilde{\mathrm{Q}}_{ij}/\mathrm{D}t$ (green, center column), and the contribution to shear by T1 transitions $\tilde{\mathrm{V}}_{ij}$ (red, right column) at different times during pupal development. The bars indicate the local axis and strength of shear averaged in a small square. The full dynamics of these patterns can be seen in the Movies M1–M3 [30]. Because here we do not track cells but use a lab frame relative to which the tissue moves, convective terms have been taken into account (see Appendix B 2). The patterns in Fig. 10 correspond to Figure 5 and Video 6 in ref. [6]. The pattern of tissue shear rate is splayed and decreases in magnitude over time. The pronounced inhomogeneities of the shear pattern at 22 hAPF are due to different behaviors of veins and the intervein regions [8]. The orientations of the patterns of cell elongation change and shear by T1 transitions are both approximately homogeneous at early and late times. At intermediate times, about 22 hAPF, a reorientation of these patterns occurs, which corresponds to a transitions between a phase I and a phase II of tissue remodeling [3, 6]. During phase I, cells elongate along the proximal-distal axis of the wing while they are undergoing T1 transitions along the anterior-posterior axis of the wing. During phase II, cells reduce their elongation along the proximal-distal axis while undergoing T1 transitions along this axis.

These dynamics and the two phases can be analyzed by averaging contributions to tissue shear in distinct subregions of the wing (see Fig. 11A) and in the whole wing blade. We project the tensorial quantities on the x axis, which is the average axis of cell elongation and is close to the proximal-distal axis (see Fig. 11B). The quantities discussed are listed in Fig. 11C. The shear rates as a function of time and the corresponding cumulative shear are shown in Fig. 11D and E, respectively, averaged over the whole wing blade. These data are consistent with the previous analysis [6]. The fact that the sum of cellular

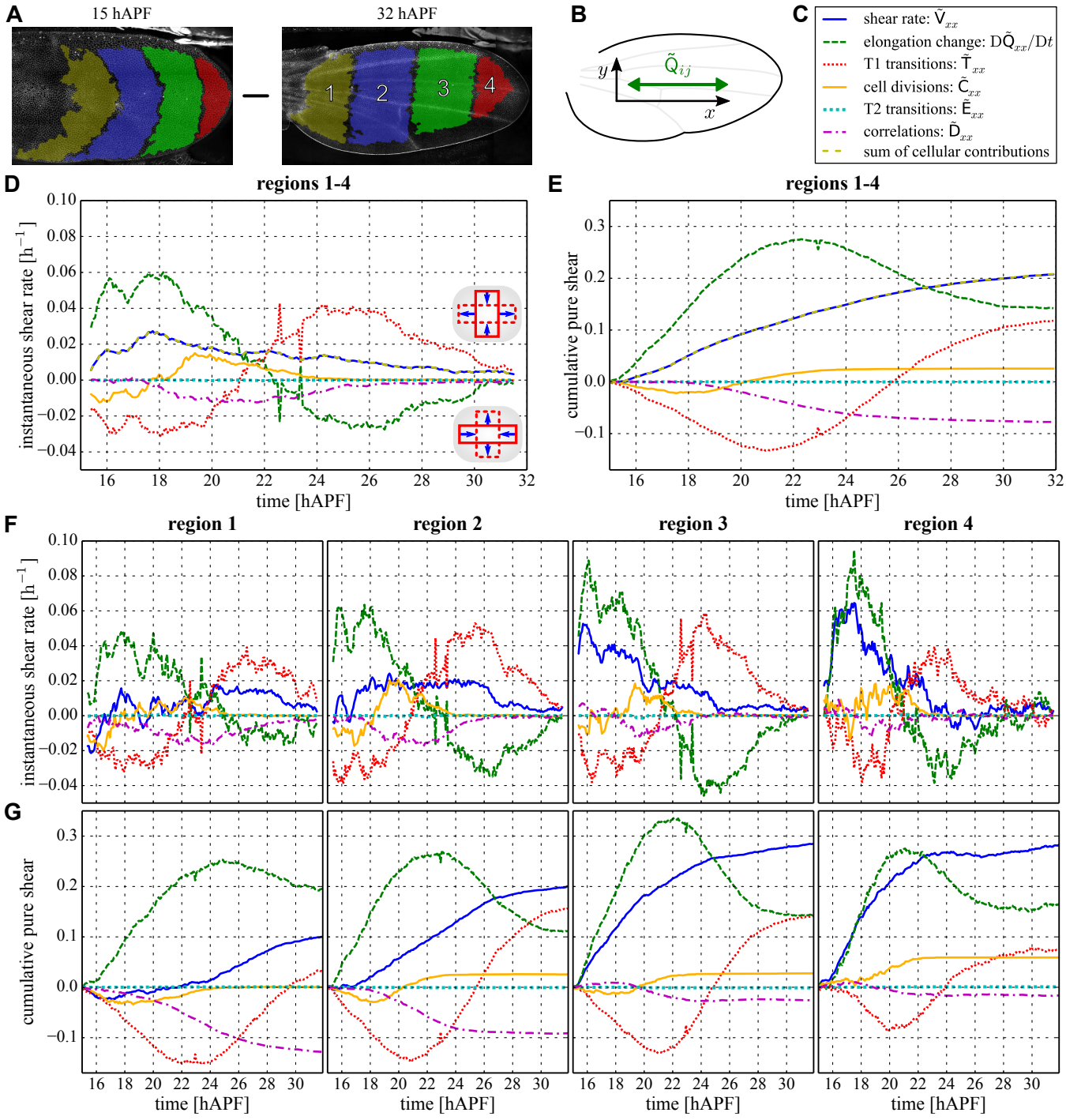

FIG. 11. Contributions to tissue shear as a function of time during pupal development of the fly wing. Shown is the data for one wing. (A) The fly wing undergoes complex tissue remodeling, which we recorded between 15 and 32 hAPF. The colored areas mark regions of tissue in which all cells were tracked during this time interval. (B) Schematic representation of the coordinate system used to describe tissue deformations. The x axis points towards the tip of the wing and is aligned parallel to the axis of cell elongation averaged within the interval between 24 and 32 hAPF and over all four regions. The average cell elongation computed for a single region deviates at most by 5 degrees from this x axis. (C) Legend specifying different contributions to tissue shear. (D) Cellular contributions to shear and total shear rate averaged over regions 1-4 in panel A as a function of time. Plotted are the projections of the tensors on the x axis, for example the component $\tilde{V}_{xx}$ of the tissue shear rate. (E) Cumulative tissue shear and cellular contributions, projected on the x axis. (F,G) Same plots as in D and E, but for the subregions 1 to 4 indicated in panel A. In D-G, data was averaged over 10 subsequent inter-frame intervals.

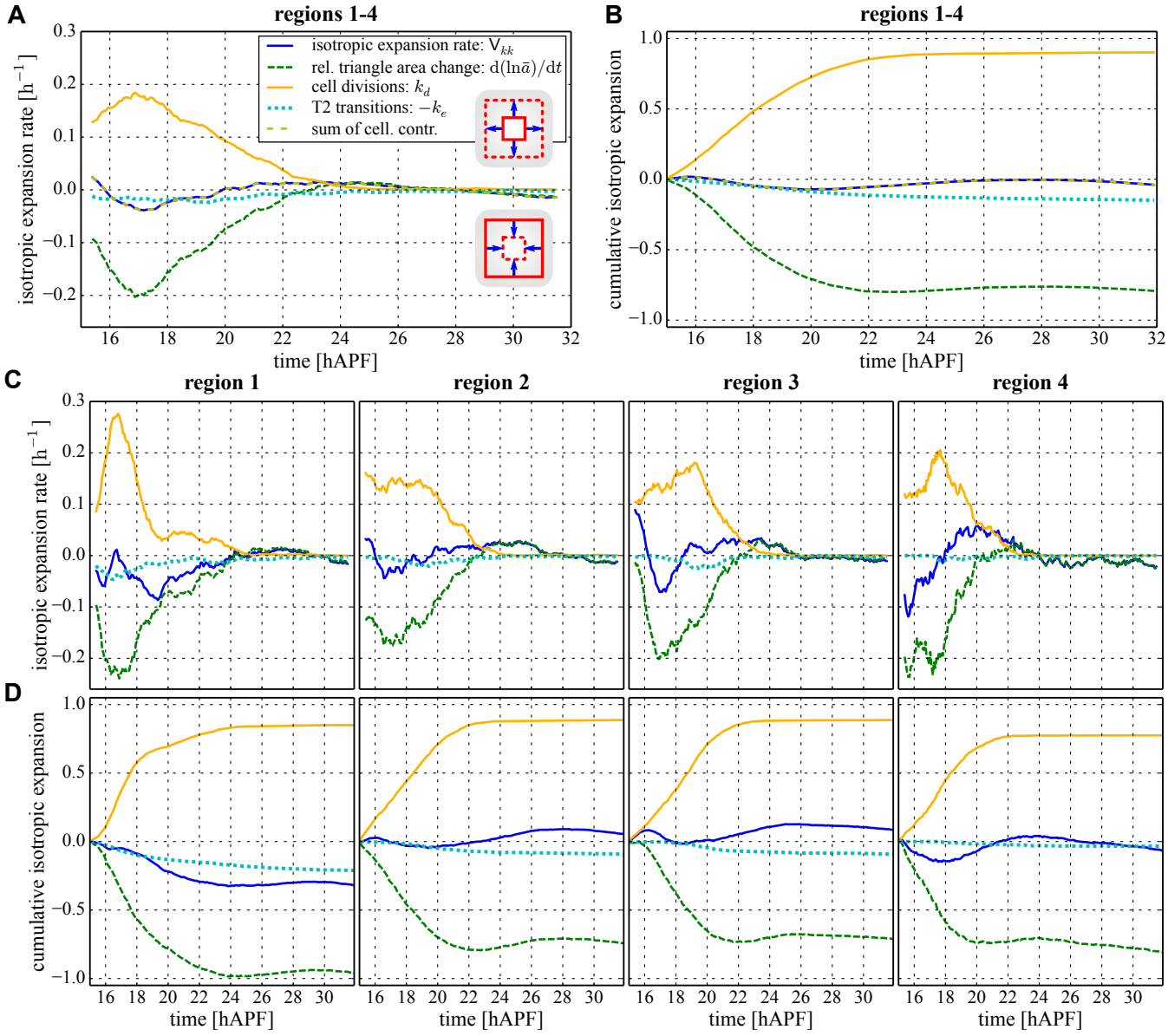

FIG. 12. Contributions to isotropic tissue expansion as a function of time during pupal development of the fly wing. Shown is the data for one wing. (A) Large-scale isotropic expansion rate and cellular contributions to it averaged over regions 1-4 as a function of time. (B) Cumulative isotropic expansion rate and cellular contributions to it. (C,D) Same plots as in A and B, but for the subregions 1 to 4 indicated in Fig. 11A. The legend in panel A applies to panels B-D, too. In all panels, data was averaged over 10 subsequent inter-frame intervals.

contributions and tissue shear coincide in panels D and E confirms the validity of Eq. (42) (solid blue and dashed yellow lines).

In panels F and G, we show shear rates and cumulative shear for the four subregions of the wing blade indicated in Fig. 11A and tracked in Movie M4 [31]. Comparing the average shear curves in Fig. 11F,G, we find systematic differences among the different regions. Most significantly, distal regions, which are regions closer to the tip of the wing (regions 3,4) shear more at early times, whereas proximal regions, i.e. regions closer to the hinge (regions 1,2), shear more towards the end of the process (solid blue curves). Moreover, the cumulative shear at the end of the process is generally larger in distal regions than in proximal regions. The transition from phase I to phase II can be seen in all four regions. However, it shifts from about 20.5 hAPF in region 4 to about 23 hAPF in region 1 (see for example intersection of dotted red and dashed green curves in panel F). Finally, cell divisions contribute more to shear distally (region 4), whereas correlations effects contribute more to shear proximally (region 1). All of these results, which we found consistently for the three analyzed wings, reveal a propagation of morphogenetic events through the tissue.

We also quantified the isotropic expansion rate V_{kk} and its cellular contributions, related by Eq. (46). For the entire wing (Fig. 12A,B), we again confirm our earlier results reported in [6]. We find that the total area of the wing blade barely changes (solid blue curve). Correspondingly, cell area decrease (dashed green curve) together with contributions from cell extrusions (dotted cyan curve) compensate most of the area changes due to cell divisions (solid orange curve). When comparing the regions 1-4 (Fig. 12C,D), area changes due to divisions occur earlier in region 1 and during a shorter time as compared to regions 2-4. Furthermore, region 1 does substantially shrink, whereas regions 2-4 barely change their areas. This difference may be related to the fact that the wing hinge contracts its area during this process. All of these results are again consistent among the three analyzed wings.

VII. DISCUSSION

In this article, we present a geometric analysis of tissue remodeling in two dimensions based on a triangulation of the cellular network. We decompose the pure shear rate, the isotropic expansion rate, and the rotation rate of the tissue into cellular contributions. The main result of this article is given by Eqs. (42) and (46). Eq. (42) provides an exact expression of the large-scale shear rate as a sum of distinct cellular contributions, stemming from cell shape changes, T1 transitions, cell divisions, cell extrusions, and from correlation effects. This decomposition is based on the fact that for a single triangle, shear deformations are related to cell elongation changes in a corotating reference frame, see Eq. (23). The corotating reference frame ensures that elongation changes associated with pure rotations do not give rise to shear deformations. In the absence of rotations, small elongation changes and shear deformations are the same. Because of nonlinearities in the corotational time derivative, the average time derivative and the time derivative of the average differ (see Eq. (34)). When coarse-graining, this gives rise to correlation contributions to tissue shear. Such correlation terms exist when tissue remodeling is spatially inhomogeneous. For example, inhomogeneities of rotation rates give rise to correlation contributions to tissue shear that stem from correlations between rotation rates and triangle elongation (see Eq. (31)). Similarly, correlations between area changes and elongation also contribute to shear. Thus, correlation contributions to large-scale tissue shear are a generic feature resulting from the interplay of nonlinearities and fluctuations. Relationships between the key quantities that underlie the decomposition of deformations are illustrated in Fig. 13.

We have recently studied tissue morphogenesis in the pupal wing epithelium using our triangle method both in fixed reference frames and reference frames comoving with the tissue [6]. During pupal morphonesesis, the wing blade elongates along the proximal-distal axis while keeping its area approximately constant. This process can be divided in two phases [3]. In the first phase, cells elongate more than the overall tissue does. This strong cell elongation is driven by active T1 transitions expanding perpendicular to the proximal-distal axis. The cell elongation then subsequently relaxes during phase two by T1 transitions along the proximal-distal axis. At late times, the tissue reaches a state with slightly elongated cells, which is a signature of active T1 transitions. Also note that our analysis has shown that correlations contribute to tissue shear. In particular, we have shown that correlations between fluctuations of rotations and cell elongations occur and play a significant role for tissue morphogenesis. Our method can therefore detect biologically relevant processes that are otherwise difficult to spot.

In the present article, we provide a refined analysis of these previously presented data, confirming our earlier findings. In addition, we perform a regional analysis of pupal wing remodeling. Discussing the shear and cellular contributions to shear of the whole wing blade and in four different subregions, we find that the main morphogenetic processes of the wing [3, 6] are also reflected in the different subregions. However, the timing of these morphogenetic processes differs among the regions, revealing a propagation of morphogenetic events through the tissue.

Our work is related to other studies that decompose tissue shear into cell deformation and cell rearrangements [13–18]. Our approach differs from these studies in that it provides an exact relation between cellular processes and tissue deformation gradients on all scales (for details see Appendix C). Recently, a method based on cell center connection lines rather than triangles was presented [18]. While ref [18] and the method presented here both provide a decomposition of shear into cellular contributions, the method presented here has an important property. We relate tissue deformations on all length scales to cellular contributions, taking into account correlation terms. Simple area-weighted averaging of triangle-based quantities generates in our approach the corresponding coarse-grained quantities on large scales (see Appendix C). Note that our approach can also be applied to finite deformations (see Appendix B).

We have focused our discussion on tissue deformations that are planar. It will be interesting to generalize our approach to curved surfaces and to bulk three-dimensional tissues. A generalization to three dimensions can be obtained by following the same ideas, but using tetrahedra as geometric elements. Most equations presented here apply also for bulk three dimensional tissues. Only Eqs. (15) and (19) require special consideration of tetrahedral geometry.

The Triangle Method described here provides a general framework to study the deformations and remodeling of cellular material. These include not only biological tissues but also complex fluid such as foams and amorphous solids. Our approach can thus provide fundamental insight into the geometry and help to understand complex

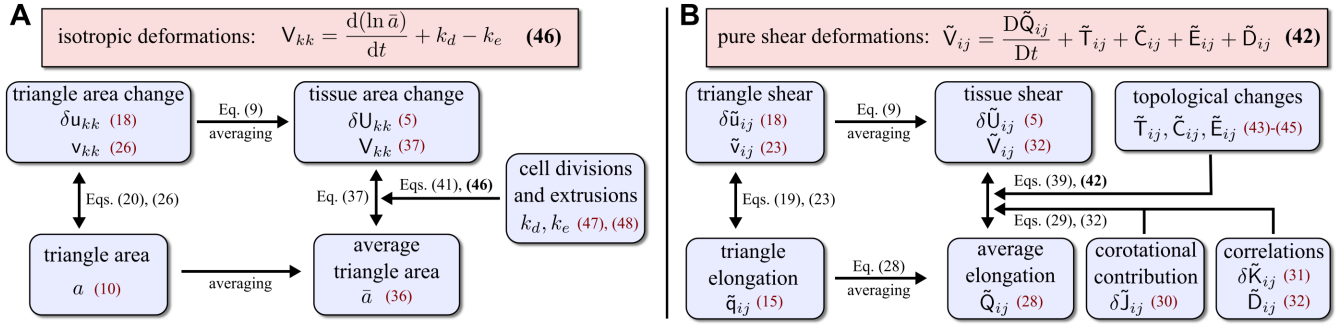

FIG. 13. Decomposition of deformations in cellular contributions. Key quantities and their relationships are shown as a schematic diagram. (A) Decomposition of the isotropic deformation rate into cellular contributions. (B) Decomposition of the pure shear rate into cellular contributions. Red numbers indicate the definition of the respective quantity (or the equation where the quantity first appears). Black numbers indicate important relations between the quantities.

rheology of cellular and amorphous materials, both living and non-living.

ACKNOWLEDGEMENTS

This work was supported by the Max Planck Gesellschaft and by the BMBF. MM also acknowledges funding from the Alfred P. Sloan Foundation, the Gordon and Betty Moore Foundation, and NSF-DMR-1352184. RE acknowledges a Marie Curie fellowship from the 774 EU 7th Framework Programme (FP7). SE acknowledges funding from the ERC.

Appendix A: Deformation of a triangle network

1. Deformation and deformation gradients

For an Eucledian space, the following equation holds for a vector field $\boldsymbol{h}$:

$$\int_\Lambda \partial_i h_j \, \mathrm{d}A = \oint_{\partial\Lambda} h_j \nu_i \, \mathrm{d}\ell, \tag{A1}$$

where the area integral is over a domain Λ with boundary $\partial\Lambda$. The vector $\boldsymbol{\nu}$ denotes the local unit vector that is normal to the boundary pointing outwards.

Eq. (A1) follows from Gauss' theorem:

$$\int_\Lambda \operatorname{div} \boldsymbol{a} \, \mathrm{d}A = \oint_{\partial\Lambda} \boldsymbol{a} \cdot \boldsymbol{\nu} \, \mathrm{d}\ell, \tag{A2}$$

if the components of the vector $\boldsymbol{a}$ are chosen as

$$a_k = \delta_{ik} h_j \tag{A3}$$

and i, j are fixed.

2. Triangulation of a cellular network

Triangulation procedure

Here, we define the triangulation procedure outlined in Section II D more precisely. An *inner* vertex, i.e. a vertex that does not lie on the margin of the polygonal network, gives rise to one or several triangles. Any inner vertex touches at least three polygons. An inner vertex that touches exactly three polygons α, β, and γ gives rise to a single triangle with corners $\boldsymbol{r}^\alpha$, $\boldsymbol{r}^\beta$, and $\boldsymbol{r}^\gamma$, as explained in Section II D. Moreover, an inner vertex that touches M with $M > 3$ polygons $\alpha_1, \ldots, \alpha_M$ gives rise to M triangles, which are defined as follows. One corner of each of these M triangles is defined by the average position $\boldsymbol{c} = (\alpha_1 + \cdots + \alpha_M)/M$. The other two corners of triangle i with $1 \le i \le M$ are defined by $\boldsymbol{r}^{\alpha_i}$ and $\boldsymbol{r}^{\alpha_{i+1}}$, where the index $i = M + 1$ corresponds to the index $i = 1$.

All non-inner vertices, i.e. those lying on the margin of the polygonal network, do not give rise to any triangles. As a result of that, a stripe along the margin of the polygonal network is not covered by triangles, which is ca. half a cell-diameter thick.

Apart from this stripe, the resulting triangulation has no gaps between the triangles. Overlaps between the triangles are in principle possible. In such a case, at least one triangle can be assigned a negative area. However in our experimental data, such cases are very seldom.

Effective number of triangles

We compute the effective number N of triangles a follows:

$$N = \sum_{n \in V_{=3}} 1 + \sum_{n \in V_{>3}} (M_n - 2). \tag{A4}$$

Here, $V_{=3}$ denotes the set of all inner three-fold vertices and $V_{>3}$ denotes the set of all inner M-fold vertices with

$M > 3$. The number M_n is the number of cells touched by vertex n (i.e. vertex n is M_n-fold). Hence, all triangles arising from a three-fold vertex count as one effective triangle, and all M triangles arising from a M-fold vertex with $M > 3$ count as $(M-2)/M$ effective triangles.

An interpretation for this effective number N of triangles is given by the following consideration. An M-fold vertex with $M > 3$ can be thought of as $M-2$ three-fold vertices that are so close to each other that they can not be distinguished from each other. If we transform each inner M-fold vertex with $M > 3$ of our polygonal network into such $M-2$ three-fold vertices, then N is the number of inner three fold-vertices in the resulting network. Put differently, N is the number of triangles in the triangulation of the resulting network.

3. Triangle shape

Side vectors of the reference triangle

In a Cartesian coordinate system, the vectors $\boldsymbol{c}^{\langle\alpha\beta\rangle}$ describing the equilateral reference triangle are

$$\boldsymbol{c}^{\langle 12\rangle} = c_0 \begin{pmatrix} 1 \\ 0 \end{pmatrix}, \tag{A5}$$

$$\boldsymbol{c}^{\langle 23\rangle} = c_0 \begin{pmatrix} -1/2 \\ \sqrt{3}/2 \end{pmatrix}, \tag{A6}$$

$$\boldsymbol{c}^{\langle 31\rangle} = c_0 \begin{pmatrix} -1/2 \\ -\sqrt{3}/2 \end{pmatrix}. \tag{A7}$$

Here, $c_0 = 2a_0^{1/2}/3^{1/4}$ is the side length and a_0 the area of the reference triangle.

Extraction of shape properties from the triangle shape transformation tensor

Here, we show how to extract triangle area a, triangle elongation $\tilde{\mathsf{q}}_{ij}$, and triangle orientation angle θ from the shape transformation tensor s_{ij} according to Eq. (15):

$$\mathsf{s} = \left(\frac{a}{a_0}\right)^{1/2} \exp(\tilde{\mathbf{q}}) \cdot \mathbf{R}(\theta). \tag{A8}$$

First, the area can be extracted by computing the determinant of this equation, which yields:

$$a = a_0 \det \mathsf{s}. \tag{A9}$$

To compute $\tilde{\mathsf{q}}_{ij}$ and θ, it is useful to split the tensor s_{ij} into a symmetric, traceless part $\tilde{\mathsf{s}}_{ij}$ and into a rest h_{ij} containing the trace and the antisymmetric part:

$$\mathsf{s}_{ij} = \tilde{\mathsf{s}}_{ij} + \mathsf{h}_{ij}. \tag{A10}$$

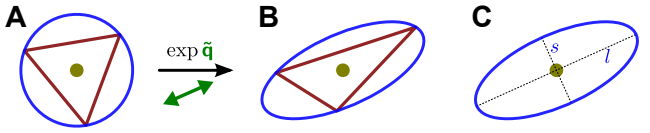

FIG. 14. Geometrical interpretation of the elongation tensor $\tilde{\mathsf{q}}_{ij}$ for a given triangle. (A) shows an equilateral triangle (red) with circumscribed circle (blue) and centroid (i.e. center of mass, yellow). (B) This triangle is deformed by the pure shear deformation given by $\exp(\tilde{\mathbf{q}})$, where $\tilde{\mathsf{q}}_{ij}$ is the elongation tensor of the so-created triangle. The former circumscribed circle is transformed to an ellipse (blue), and the former centroid is still the centroid of both the triangle and the ellipse (yellow). (C) Long and short axes of the ellipse with lengths l and s, respectively.

Then, the triangle orientation angle θ is such that h_{ij} corresponds to a rotation by θ up to a scalar factor f:

$$\mathsf{h}_{ij} = f\mathsf{R}_{ij}(\theta), \tag{A11}$$

and the triangle elongation can be computed as:

$$\tilde{\mathsf{q}}_{ij} = \frac{1}{|\tilde{\mathsf{s}}|} \operatorname{arcsinh}\left[\left(\frac{a}{a_0}\right)^{-1/2} |\tilde{\mathsf{s}}|\right] \tilde{\mathsf{s}}_{ik}\mathsf{R}_{kj}(-\theta). \tag{A12}$$

In [22], we show that these values for a, $\tilde{\mathsf{q}}_{ij}$, and θ do indeed fulfill Eq. (A8), and that they are the unique solutions.

Geometrical interpretation of the triangle elongation tensor

Fig. 14 illustrates the geometrical interpretation of the triangle elongation tensor $\tilde{\mathsf{q}}_{ij}$. Take the unique ellipse (blue in Fig. 14B) that goes through all three corners of the triangle (red) and has the same center of mass (yellow) as the triangle. Then, the long axis of the ellipse corresponds to the axis of the triangle elongation tensor $\tilde{\mathsf{q}}_{ij}$, and the aspect ratio of the ellipse is given by $l/s = \exp(2|\tilde{\mathsf{q}}|)$ (Fig. 14C).

This can be seen as follows. As discussed in Section III A and the previous section, any given triangle can be created out of an equilateral triangle using the pure shear transformation $\exp(\tilde{\mathbf{q}})$, where $\tilde{\mathsf{q}}_{ij}$ is the elongation tensor of the given triangle. This is illustrated in Fig. 14A-B. The circumscribed circle of the equilateral triangle transforms into the ellipse via the pure shear transformation. Thus, the length of the long and short axes of the ellipse are $l = r\exp(|\tilde{\mathsf{q}}|)$ and $s = r\exp(-|\tilde{\mathsf{q}}|)$, where r is the radius of the circle.

The ellipse is uniquely defined, because the equilateral triangle and the pure shear deformation are uniquely defined as proven in [22]. If there was another ellipse that went through all corners of the triangle and had the same center of mass, this ellipse could be created from a circle c' using a different pure shear transformation. Applying the inverse of this pure shear transformation to the actual triangle n would yield a triangle n'. Obviously, the

triangle n' would have the circumscribed circle c' and thus its center of mass would coincide with the center of its circumscribed circle c'. Thus, n' would be equilateral. However, this is not possible since there is only one equilateral triangle from which triangle n can emerge by a pure shear deformation.

4. Relation between triangle shape and triangle deformation

Here, we derive Eqs. (19)–(21) in the main text. From Eq. (17) follows with Eq. (8):

$$\mathsf{s}'_{ij} - \mathsf{s}_{ij} = \mathsf{u}_{ki}\mathsf{s}_{kj}. \tag{A13}$$

For infinitesimal changes $\delta\tilde{\mathsf{q}}_{ij}$, δa, $\delta\theta$ of the respective triangle shape properties, the difference of the shape transformation tensors is also infinitesimal $\delta\mathsf{s}_{ij} = \mathsf{s}'_{ij} - \mathsf{s}_{ij}$. From Eq. (A8) follows:

$$\begin{aligned}\delta\mathsf{s}_{ij} = \frac{\delta a}{2a}\mathsf{s}_{ij} + \delta|\tilde{\mathsf{q}}|\frac{\tilde{\mathsf{q}}_{ik}}{|\tilde{\mathsf{q}}|}\mathsf{s}_{kj} + \delta\phi\epsilon_{ik}\mathsf{s}_{kj} \\ + (\delta\theta - \delta\phi)\mathsf{s}_{ik}\epsilon_{kj}.\end{aligned} \tag{A14}$$

Inserted into Eq. (A13) and using the decomposition of the deformation tensor Eq. (5), this yields:

$$\begin{aligned}&\frac{1}{2}\delta\mathsf{u}_{kk}\delta_{ij} + \delta\tilde{\mathsf{u}}_{ij} + \delta\psi\epsilon_{ij} \\ &= \frac{\delta a}{2a}\delta_{ij} + \delta|\tilde{\mathsf{q}}|\frac{\tilde{\mathsf{q}}_{ij}}{|\tilde{\mathsf{q}}|} + \delta\phi\epsilon_{ij} \\ &\quad + (\delta\theta - \delta\phi)\mathsf{s}_{ik}\epsilon_{kl}\mathsf{s}^{-1}_{lj}.\end{aligned} \tag{A15}$$

To disentangle the contributions of the last term to the three deformation tensor components, we transform the tensor product into:

$$\mathsf{s}_{ik}\epsilon_{kl}\mathsf{s}^{-1}_{lj} = \epsilon_{ik}\left[\cosh(2|\tilde{\mathsf{q}}|)\delta_{kj} - \frac{\sinh(2|\tilde{\mathsf{q}}|)}{|\tilde{\mathsf{q}}|}\tilde{\mathsf{q}}_{kj}\right]. \tag{A16}$$

Hence, we obtain:

$$\delta\tilde{\mathsf{u}}_{ij} = \delta|\tilde{\mathsf{q}}|\frac{\tilde{\mathsf{q}}_{ij}}{|\tilde{\mathsf{q}}|} - (\delta\theta - \delta\phi)\frac{\sinh(2|\tilde{\mathsf{q}}|)}{|\tilde{\mathsf{q}}|}\epsilon_{ik}\tilde{\mathsf{q}}_{kj} \tag{A17}$$

$$\delta\mathsf{u}_{kk} = \frac{\delta a}{a} \tag{A18}$$

$$\delta\psi = \delta\phi + (\delta\theta - \delta\phi)\cosh(2|\tilde{\mathsf{q}}|). \tag{A19}$$

Eqs. (19)–(21) in the main text follow directly. Note that Eqs. (A17)–(A19) can be rewritten into:

$$\delta\tilde{\mathsf{u}}_{ij} = \delta\tilde{\mathsf{q}}_{ij} - 2\Big[c\delta\psi + (1-c)\delta\phi\Big]\epsilon_{ik}\tilde{\mathsf{q}}_{kj} \tag{A20}$$

$$\delta\mathsf{u}_{kk} = \delta(\ln a) \tag{A21}$$

$$\delta\psi = \delta\theta - \delta\tilde{\mathsf{u}}_{ij}\epsilon_{jk}\tilde{\mathsf{q}}_{ki}\frac{\cosh(2|\tilde{\mathsf{q}}|) - 1}{2|\tilde{\mathsf{q}}|\sinh(2|\tilde{\mathsf{q}}|)}. \tag{A22}$$

with $c = \tanh(2|\tilde{\mathsf{q}}|)/2|\tilde{\mathsf{q}}|$. Here, to derive the expression for the pure shear part $\delta\tilde{\mathsf{u}}_{ij}$, we used the decomposition of $\delta\tilde{\mathsf{q}}_{ij}$ into contributions of norm and angle changes of $\tilde{\mathsf{q}}_{ij}$, Eq. (A24). To derive the expression for the rotation part $\delta\psi$, we used that that from Eq. (A17) follows that:

$$\delta\tilde{\mathsf{u}}_{ij}\epsilon_{jk}\tilde{\mathsf{q}}_{ki} = -2(\delta\theta - \delta\phi)|\tilde{\mathsf{q}}|\sinh(2|\tilde{\mathsf{q}}|). \tag{A23}$$

Pure shear by triangle elongation change

To discuss the pure shear formula Eq. (A20), we first consider the decomposition of an infinitesimal change of the triangle elongation tensor $\delta\tilde{\mathsf{q}}_{ij}$ into a contribution by the change of the norm $\delta|\tilde{\mathsf{q}}|$ and a contribution by the change of the angle $\delta\phi$:

$$\delta\tilde{\mathsf{q}}_{ij} = \delta|\tilde{\mathsf{q}}|\frac{\tilde{\mathsf{q}}_{ij}}{|\tilde{\mathsf{q}}|} + 2\delta\phi\epsilon_{ik}\tilde{\mathsf{q}}_{kj}. \tag{A24}$$

The pure shear $\delta\tilde{\mathsf{u}}_{ij}$ from Eq. (A20) can be rewritten in a similar form:

$$\delta\tilde{\mathsf{u}}_{ij} = \delta|\tilde{\mathsf{q}}|\frac{\tilde{\mathsf{q}}_{ij}}{|\tilde{\mathsf{q}}|} + 2c(\delta\phi - \delta\psi)\epsilon_{ik}\tilde{\mathsf{q}}_{kj}. \tag{A25}$$

There are two differences between Eq. (A24) and Eq. (A25) both of which affect the angular part. First, in Eq. (A25), the rotation $\delta\psi$ is subtracted from the angular change of the elongation tensor, $\delta\phi$. This accounts for bare rotations, which do change the elongation tensor $\tilde{\mathsf{q}}_{ij}$ by changing its angle ϕ, but do not contribute to pure shear $\delta\tilde{\mathsf{u}}_{ij}$. Second, the "rotation-corrected" angle change of the elongation tensor, $\delta\phi - \delta\psi$, does not fully contribute to pure shear but is attenuated by a factor c with $0 < c \leq 1$, which depends nonlinearly on $|\tilde{\mathsf{q}}|$. This second point makes the corotational time derivative in Eq. (24) different from other, more common time derivatives. However, for small elongations, $|\tilde{\mathsf{q}}| \ll 1$, we have $c \to 1$ and the corotational time derivative corresponds to the so-called Jaumann derivative [24].

Shear-induced triangle rotation

Here, we discuss the shear-induced contribution $\delta\xi$ in Eq. (A22), which we rewrite as

$$\delta\theta = \delta\psi + \delta\xi \tag{A26}$$

with

$$\delta\xi = \delta\tilde{\mathsf{u}}_{ij}\epsilon_{jk}\tilde{\mathsf{q}}_{ki}\frac{\cosh(2|\tilde{\mathsf{q}}|) - 1}{2|\tilde{\mathsf{q}}|\sinh(2|\tilde{\mathsf{q}}|)}. \tag{A27}$$

According to this equation, the triangle orientation angle θ may change even with vanishing $\delta\psi$ whenever there is pure shear that is neither parallel nor perpendicular to the elongation tensor $\tilde{\mathsf{q}}_{ij}$, i.e. a pure shear that changes the elongation angle.

We illustrate this further in Fig. 15. For clarity, we use a Minerva head in place of a triangle, but with

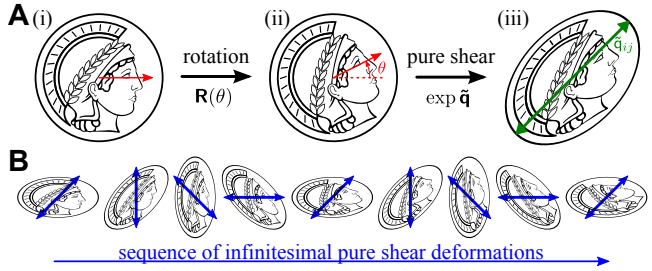

FIG. 15. Illustration of the shear-induced rotation effect $\delta\xi$ appearing in Eq. (A22). For clarity, we use a Minerva head in place of a triangle. (A) The definitions of orientation angle θ and elongation tensor $\tilde{\mathsf{q}}_{ij}$ are analogous to the triangle quantities (Fig. 4C). Roughly, the orientation angle θ corresponds to the direction in which the Minerva head looks. The isotropic scaling has been set to one for simplicity ($a = a_0$). (B) The elongated Minerva head is subject to a continuous pure shear deformation with varying shear axis. The pure shear axis is at each time point oriented with an angle of $\pi/4$ with respect to the elongation axis ϕ, such that the elongation norm $|\tilde{\mathsf{q}}|$ does not change but only the angle ϕ. Here, snapshots of such a deformation are shown. Alternatively, Movie M5 shows this deformation more smoothly [a]. Strikingly, the head orientation angle θ changes by this deformation although the deformation never includes any rotation component $\delta\psi = 0$. Here, we have set $|\tilde{\mathsf{q}}| = (\ln 2)/2$ such that $\delta\theta = \delta\xi = 0.2\delta\phi$.

[a] See Supplemental Material at [URL will be inserted by publisher]

analogously defined shape and deformation properties (Fig. 15A). We discuss a continuous pure shear deformation of this head without rotation or isotropic expansion at any time point (Fig. 15B):

$$\delta\mathsf{u}_{kk} = 0 \tag{A28}$$
$$\delta\psi = 0. \tag{A29}$$

Because of Eq. (A29), any potential change in the orientation angle θ must be due to the shear-induced effect: $\delta\theta = \delta\xi$. Furthermore, the pure shear is defined such that the elongation norm $|\tilde{\mathsf{q}}|$ is constant, but the elongation angle ϕ may change. This can be accomplished by a pure shear axis that is at each time point at an angle of $\pi/4$ with respect to the elongation axis. This criterion can be written as:

$$\delta\tilde{\mathsf{u}}_{ij} = \delta h \epsilon_{ik}\tilde{\mathsf{q}}_{kj}, \tag{A30}$$

where δh is some infinitesimal scalar quantity. Comparison of this equation with Eq. (A20) and insertion into Eq. (A27) yields:

$$\delta\xi = \delta\phi\left[1 - \frac{1}{\cosh(2|\tilde{\mathsf{q}}|)}\right]. \tag{A31}$$

Hence, although there is no rotation component of the deformation field $\delta\psi = 0$, the orientation angle θ changes by a non-vanishing amount $\delta\theta = \delta\xi$ (Fig. 15B, Movie M5 [32]).

5. Large-scale pure shear

Relation to average elongation

To find the relation between large-scale pure shear $\delta\tilde{\mathsf{U}}_{ij}$ and large-scale elongation $\tilde{\mathsf{Q}}_{ij}$, we average Eq. (19):

$$\delta\tilde{\mathsf{U}}_{ij} = \langle\delta\tilde{\mathsf{q}}_{ij}\rangle + \langle\delta\tilde{\mathsf{j}}_{ij}\rangle. \tag{A32}$$

To show Eq. (29), it remains to be shown that:

$$\delta\tilde{\mathsf{Q}}_{ij} = \langle\delta\tilde{\mathsf{q}}_{ij}\rangle + \langle\delta\mathsf{u}_{kk}\tilde{\mathsf{q}}_{ij}\rangle - \delta\mathsf{U}_{kk}\tilde{\mathsf{Q}}_{ij}. \tag{A33}$$

This equation reflects the fact that changes in the triangle areas also contribute to a change in the average elongation $\tilde{\mathsf{Q}}_{ij}$. Formally, the equation can be derived using the definition of the average elongation $\tilde{\mathsf{Q}}_{ij} = \langle\tilde{\mathsf{q}}_{ij}\rangle$ together with Eqs. (20) and (36).

Alternative definition for the mean-field corotational term

In Eq. (30) we have introduced a mean-field corotational term $\delta\tilde{\mathsf{J}}_{ij}$ to account for global rotations, which do not contribute to the overall pure shear rate, but change the average elongation tensor $\tilde{\mathsf{Q}}_{ij}$. We use the definition Eq. (30) throughout this article. However, note that there are different conventions possible for $\delta\tilde{\mathsf{J}}_{ij}$. While the definition Eq. (30) was chosen in analogy to Eq. (24), one could alternatively define based on Eq. (22):

$$\delta\tilde{\mathsf{J}}_{ij} = -2\Big[G\delta\Theta + (1-G)\delta\Phi\Big]\epsilon_{ik}\tilde{\mathsf{Q}}_{kj}, \tag{A34}$$

where $G = \sinh(2|\tilde{\mathsf{Q}}|)/2|\tilde{\mathsf{Q}}|$ and $\delta\Theta = \langle\delta\theta\rangle$. Note that both definitions, Eq. (30) and Eq. (A34), yield in general different values for $\delta\tilde{\mathsf{J}}_{ij}$.

Correlation terms arising from convective and corotational terms

Here, we show how the correlation term $\tilde{\mathsf{D}}_{ij}$ arises from convective and corotational terms. To this end, we introduce continuous, time-dependent fields for shear rate $\tilde{v}_{ij}(\boldsymbol{r},t)$ and triangle elongation $\tilde{Q}_{ij}(\boldsymbol{r},t)$. Whenever a given position $\boldsymbol{r}$ lies inside of a triangle n at time point t, both are defined by:

$$\tilde{v}_{ij}(\boldsymbol{r},t) = \tilde{\mathsf{v}}^n_{ij} \tag{A35}$$
$$\tilde{Q}_{ij}(\boldsymbol{r},t) = \tilde{\mathsf{q}}^n_{ij}. \tag{A36}$$

Given these definitions, Eq. (23) can be rewritten as:

$$\tilde{v}_{ij} = \frac{\mathcal{D}\tilde{Q}_{ij}(\boldsymbol{r},t)}{\mathcal{D}t} \tag{A37}$$

with the corotational time derivative $\mathcal{D}\tilde{Q}_{ij}/\mathcal{D}t$ defined as

$$\frac{\mathcal{D}\tilde{Q}_{ij}}{\mathcal{D}t} = \frac{\partial\tilde{Q}_{ij}(\boldsymbol{r},t)}{\partial t} + \mathsf{v}_k\partial_k\tilde{Q}_{ij} + \frac{\delta\tilde{\mathsf{j}}^n_{ij}}{\delta t}. \tag{A38}$$

Here, n is the triangle which contains the position $\boldsymbol{r}$ at time t. The vector v_k denotes the velocity field that is obtained by linear interpolation between the cell center velocities, i.e. by $\mathbf{v}(\boldsymbol{r})\delta t = \boldsymbol{h}(\boldsymbol{r})$ with $\boldsymbol{h}(\boldsymbol{r})$ given by Eq. (7).

In Eq. (A38), we take the corotational term $\delta\tilde{\mathsf{j}}^n_{ij}/\delta t$ directly from the triangle-related Eq. (23). However in addition, a convective term $\mathrm{v}_k\partial_k\tilde{Q}_{ij}$ needs to be introduced for the following reason. The partial time derivative $\partial\tilde{Q}_{ij}(\boldsymbol{r},t)/\partial t$ on the right-hand side is essentially different from the "total" time derivative $\delta\tilde{\mathsf{q}}^n_{ij}/\delta t$ appearing in Eq. (24): Whenever the tissue moves such that the boundary between two triangles passes past position $\boldsymbol{r}$, the partial time derivative contains a Dirac δ peak, which is not contained in the "total" time derivative. This peak is exactly compensated for by the convective term, which is only nonzero at triangle boundaries.

To obtain the large-scale shear rate of a triangulation, we can coarse-grain Eq. (A37) instead of the triangle relation Eq. (23). Eventually, we should obtain the same relation for the large-scale shear rate, Eq. (32). By comparing both ways, we can spot which term in the continuum formulation give rise to which terms in the triangle formulation.

To coarse grain Eq. (A37), we write the large-scale shear rate $\tilde{\mathsf{V}}_{ij}$ as follows (using Eq. (3)):

$$\tilde{\mathsf{V}}_{ij} = \langle\tilde{v}_{ij}\rangle, \tag{A39}$$

where the averaging bracket is defined as follows

$$\langle\tilde{v}_{ij}\rangle = \frac{1}{A}\int_\Lambda \tilde{v}_{ij}\,\mathrm{d}A. \tag{A40}$$

Here, the integration is over the whole triangle network Λ with area A. Substituting Eq. (A37) into Eq. (A39) yields:

$$\begin{aligned}\tilde{\mathsf{V}}_{ij} = \left\langle\frac{\partial\tilde{Q}_{ij}(\boldsymbol{r},t)}{\partial t}\right\rangle - \left\langle(\partial_k\mathrm{v}_k)\tilde{Q}_{ij}\right\rangle + \left\langle\frac{\delta\tilde{\mathsf{j}}_{ij}}{\delta t}\right\rangle \\ + \frac{1}{A}\oint_{\partial\Lambda}\nu_k\mathrm{v}_k\tilde{Q}_{ij}\,\mathrm{d}A.\end{aligned} \tag{A41}$$

Here, we carried out a partial integration on the term arising from the convective term, which gave rise to the boundary integral. In the boundary integral, the vector ν_k denotes the unit vector normal to the boundary, pointing outwards.

The second and the third terms in Eq. (A41) are essential parts of the correlation term $\tilde{\mathsf{D}}_{ij}$. In particular, the term $-\langle(\partial_k\mathrm{v}_k)\tilde{Q}_{ij}\rangle = -\langle\mathsf{v}_{kk}\tilde{\mathsf{q}}_{ij}\rangle$, which arose from the convective term, is an essential part of the growth correlation. Similarly, the term $\langle\delta\tilde{\mathsf{j}}_{ij}/\delta t\rangle$ is an essential part of the rotational correlation.

To obtain Eq. (32) from Eq. (A41), we note that the average elongation is $\tilde{\mathsf{Q}}_{ij} = \langle\tilde{Q}_{ij}\rangle$, and transform its total time derivative:

$$\begin{aligned}\frac{\delta\tilde{\mathsf{Q}}_{ij}}{\delta t} = \frac{1}{\delta t}\left(\frac{1}{A(t+\delta t)} - \frac{1}{A(t)}\right)\int_{\Lambda(t)}\tilde{Q}_{ij}\,\mathrm{d}A \\ + \frac{1}{A\delta t}\left(\int_{\Lambda(t+\delta t)}\tilde{Q}_{ij}\,\mathrm{d}A - \int_{\Lambda(t)}\tilde{Q}_{ij}\,\mathrm{d}A\right) \\ + \frac{1}{A\delta t}\int_{\Lambda(t)}\delta\tilde{Q}_{ij}\,\mathrm{d}A.\end{aligned} \tag{A42}$$

These three terms can be respectively transformed into:

$$\frac{\delta\tilde{\mathsf{Q}}_{ij}}{\delta t} = -\mathsf{V}_{kk}\tilde{\mathsf{Q}}_{ij} + \frac{1}{A}\int_{\partial\Lambda}\nu_k\mathrm{v}_k\tilde{Q}_{ij}\,\mathrm{d}A + \left\langle\frac{\partial\tilde{Q}_{ij}(\boldsymbol{r},t)}{\partial t}\right\rangle. \tag{A43}$$

The first term is the mean-field term in the growth correlation and the second term is the boundary term generated by the convective term. Both terms appear due to a possible change of the triangulation domain Λ. After all, Eq. (32) follows by inserting Eq. (A43) into Eq. (A41).

6. Pure shear by a single T1 transition

In the absence of T1 transitions, we have $\Delta\tilde{\mathsf{U}}_{ij} = \Delta\tilde{\mathsf{Q}}_{ij} + \Delta\tilde{\mathsf{J}}_{ij} + \Delta\tilde{\mathsf{K}}_{ij}$, which can be obtained by integrating Eq. (29) over time. Here, $\Delta\tilde{\mathsf{U}}_{ij}$ is the tissue pure shear computed using Eq. (4), $\Delta\tilde{\mathsf{Q}}_{ij}$ is the change of the average triangle elongation, and $\Delta\tilde{\mathsf{J}}_{ij}$ and $\Delta\tilde{\mathsf{K}}_{ij}$ are the corotational and correlation contributions. We now define the shear associated with the T1 transition $\Delta\tilde{\mathsf{X}}_{ij}$ such that the following decomposition holds in the presence of a single T1 transition: $\Delta\tilde{\mathsf{U}}_{ij} = \Delta\tilde{\mathsf{X}}_{ij} + \Delta\tilde{\mathsf{Q}}_{ij} + \Delta\tilde{\mathsf{J}}_{ij} + \Delta\tilde{\mathsf{K}}_{ij}$.

During a single T1 transition, two adjacent triangles are replaced by two new triangles such that the quadrilateral formed by both triangles remains unchanged (Fig. 8). In order to define the shear associated with this retriangulation, we choose a continuous deformation that transforms each of the initial triangles into one of the final triangles as follows. Each initial triangle is first deformed to an equilateral triangle by a pure shear deformation starting from the initial $\tilde{\mathsf{q}}^n_{ij}$ and arriving at $\tilde{\mathsf{q}}^n_{ij} = 0$. The resulting equilateral triangle is reoriented and rescaled such that by a subsequent pure shear deformation increasing $\tilde{\mathsf{q}}^n_{ij}$, the final triangle shape is reached. Because the quadrilateral formed by both triangles has the same shape before and after the T1 transition, $\Delta\tilde{\mathsf{U}}_{ij} = 0$. Moreover, the continuous deformation via equilateral intermediate states does not generate corotational or correlation contributions $\Delta\tilde{\mathsf{J}}_{ij} = \Delta\tilde{\mathsf{K}}_{ij} = 0$, such that we define

$$\Delta\tilde{\mathsf{X}}_{ij} = -\Delta\tilde{\mathsf{Q}}_{ij}. \tag{A44}$$

The absence of corotational and correlation contributions is consistent with the fact that the quadrilateral formed by the pair of triangles does not rotate during

the T1 transition. Note that in principle, one could also use different continuous deformations to compute $\Delta\tilde{\mathsf{Q}}_{ij} + \Delta\tilde{\mathsf{J}}_{ij} + \Delta\tilde{\mathsf{K}}_{ij}$. This would correspond to a different convention for the definition of $\Delta\tilde{\mathsf{X}}_{ij}$. In this case, corotational and correlation contributions to $\Delta\tilde{\mathsf{X}}_{ij}$ could in general occur and the definition of $\Delta\tilde{\mathsf{X}}_{ij}$ may depend on which of the initial triangles is transformed into which of the final triangles. Thus, the convention proposed here is the simplest choice, does not introduce rotational contributions, and does not depend on the association of initial to final triangles.

Note that the triangle elongation angle Φ changes during the T1 transition. Although in between T1 transitions, $\delta\Phi$ contributes to $\delta\tilde{\mathsf{J}}_{ij}$ (see Eq. (30)), the convention chosen here, $\Delta\tilde{\mathsf{J}}_{ij} = 0$, implies that the T1-induced change in Φ does not contribute to the corotational time derivative $\mathrm{D}\tilde{\mathsf{Q}}_{ij}/\mathrm{D}t$.

Special case: square or rhombus

Here, we derive the shear by a single T1 transition for the special case where the four involved cell centers (green dots in Fig. 8) form a square or, more generally, a rhombus.

For the case of a square, all involved triangles are isosceles triangles with a base angle of $\pi/4$. Such a triangle has an elongation tensor with an axis parallel to the base and with the norm $|\tilde{\mathsf{q}}^n| = (\ln 3)/4$. This can be shown using the formulas presented in Appendix A 3, or by the following reasoning. We ask for the shape transformation tensor s^n_{ij} needed to transform an equilateral reference triangle into an isosceles triangle with the same area and a base angle of $\pi/4$. We set one of the sides of the reference triangle and the base of the isosceles triangle parallel to the x axis. Then, the ratio of the base length of the isosceles triangle to the side length of the reference triangle is $3^{1/4}$, and the ratio of the heights of both triangles is $3^{-1/4}$. Correspondingly, the shape transformation tensor reads

$$\mathsf{s}^n = \begin{pmatrix} 3^{1/4} & 0 \\ 0 & 3^{-1/4} \end{pmatrix}. \tag{A45}$$

This shape transformation tensor corresponds to the elongation tensor $\tilde{\mathsf{q}}^n_{ij}$ that is parallel to the x axis and has norm $|\tilde{\mathsf{q}}^n| = (\ln 3)/4$.

The shear by the T1 transition is given by the change of the average elongation tensor. For the case of a square, both triangles before and after the T1 transition have the same elongation tensor with norm $|\tilde{\mathsf{q}}^n| = (\ln 3)/4$. Thus, also the average elongation tensors for the square before and after the T1 transition have norm $|\tilde{\mathsf{Q}}| = (\ln 3)/4$. However, the axes of both average elongation tensors are perpendicular to each other, oriented along the diagonals of the square. Thus the shear by the T1 transition, which is given by the change of the average elongation tensor has norm $|\Delta\tilde{X}| = (\ln 3)/2$.

The more general case of a rhombus can be treated by transforming the rhombus into a square by a pure shear transformation along the short diagonal of the rhombus. The effects of this pure shear transformation on the average elongation tensors before and after the T1 transition cancel out exactly. Note however that this argument only works because the axis of this pure shear transformation is parallel or perpendicular to the elongation axes of all involved triangles.

In the above arguments, the average elongation was computed only for the rhombus with area $A_\square$. However, when the triangulation under consideration extends beyond the rhombus and has area A, the norm of the shear by the T1 transition results to be $|\Delta\tilde{X}| = (A_\square \ln 3)/(2A)$.

7. Cellular contributions to isotropic expansion of a polygonal network

We derive a decomposition of the isotropic expansion rate V^p_{kk} of the polygonal network. To this end, we first define the infinitesimal deformation tensor $\delta\mathsf{U}^p_{ij}$ for the whole polygonal network using a variant of Eq. (11), where we sum over polygon edges b along the outline of the polygonal network instead of triangle sides along the outline of the triangular network:

$$\delta\mathsf{U}^p_{ij} = \frac{1}{A^p}\sum_b \delta h^b_j \nu^b_i \Delta\ell^b. \tag{A46}$$

Here, A^p is the area of the polygonal network, the vector ν^b_i is the unit vector normal to side b that points outside, the scalar $\Delta\ell^b$ is the length of side b, and $\delta h^b_j = (\delta h^m_j + \delta h^n_j)/2$ with m and n being the vertices at the ends of edge b, and δh^m_j and δh^n_j being their respective displacement vectors.

Then we have that:

$$\delta\mathsf{U}^p_{kk} = \frac{\delta A^p}{A^p}, \tag{A47}$$

where δA^p is the change of the area across the deformation. This equation can be shown using that $A^p = \sum_b r^b_k \nu^b_k \Delta\ell^b$ where the sum is over all polygon edges b along the outline of the polygonal network, $r^b_k = (r^m_k + r^n_k)/2$ with m and n being the vertices at the ends of edge b, and r^m_k and r^n_k being their respective positions.

Defining the average cell area by $\bar{a}^p = A^p/N^p$ where N^p is the number of cells in the polygonal network, we have for the case without topological transitions:

$$\delta\mathsf{U}^p_{kk} = \delta(\ln \bar{a}^p). \tag{A48}$$

Topological transitions are accounted for as explained in Section IV B. Hence, we finally obtain Eq. (49) with

$$k^p_d = \sum_{k\in\mathrm{CD}} \delta(t - t_k) \ln\left(1 + \frac{1}{N^p_k}\right) \tag{A49}$$

$$k_e^p = -\sum_{k\in \mathrm{T2}} \delta(t-t_k)\ln\left(1-\frac{1}{N_k^p}\right), \tag{A50}$$

where the sums run over all topological transitions k of the respective kind, t_k denotes the time point of the respective transition, and N_k^p is the number of cells in the network before the respective transition.

8. Cellular contributions to large-scale rotation in a triangle network

For the sake of completeness, we discuss the decomposition of large-scale rotation $\Omega = \langle\omega\rangle$, i.e. $\Omega\delta t = \delta\Psi$, into cellular contributions similar to the shear rate decomposition Eq. (42). In particular, we want to relate Ω to average triangle orientation, which we characterize using the complex hexatic order parameter P_6 with:

$$P_6 = \langle p_6\rangle \qquad \text{with} \qquad p_6 = e^{6i\theta}. \tag{A51}$$

Here, we use again an area-weighted average over all triangles, i denotes the imaginary unit, and θ is the triangle orientation angle defined in Eq. (15).

In the absence of topological transitions, the change of the hexatic order parameter P_6 relates to the large-scale rotation rate Ω as follows (using Eq. (27)):

$$\begin{aligned}\frac{\mathrm{d}P_6}{\mathrm{d}t} = {}& 6iP_6\left[\Omega + \tilde{\mathsf{V}}_{ij}\epsilon_{jk}\tilde{\mathsf{Q}}_{ki}f(|\tilde{\mathsf{Q}}|)\right]\\ &+\Big(\langle \mathsf{v}_{kk}p_6\rangle - \mathsf{V}_{kk}P_6\Big) + 6i\Big(\langle\omega p_6\rangle - \Omega P_6\Big)\\ &+6i\left(\left\langle\tilde{\mathsf{v}}_{ij}\epsilon_{jk}\tilde{\mathsf{q}}_{ki}f(|\tilde{\mathsf{q}}|)p_6\right\rangle - \tilde{\mathsf{V}}_{ij}\epsilon_{jk}\tilde{\mathsf{Q}}_{ki}f(|\tilde{\mathsf{Q}}|)P_6\right)\end{aligned} \tag{A52}$$

with $f(w) = [\cosh(2w)-1]/[2w\sinh(2w)]$.

The complex hexatic order parameter P_6 contains two pieces of information, the magnitude Z_6 of hexatic order and its orientation Θ_6, which are real numbers defined by:

$$P_6 = Z_6 e^{6i\Theta_6}. \tag{A53}$$

Here, the orientation angle is defined to lie within the interval $-\pi/6 < \Theta_6 \le \pi/6$. The value of the magnitude can be expressed as the average $Z_6 = \langle\cos(6[\theta-\Theta_6])\rangle$. Using Eq. (A53), Eq. (A52) splits into an equation for the magnitude:

$$\begin{aligned}\frac{\mathrm{d}Z_6}{\mathrm{d}t} = {}&\Big\langle \mathsf{v}_{kk}\cos(6[\theta-\Theta_6])\Big\rangle - \mathsf{V}_{kk}Z_6\\ &-6\Big\langle\omega\sin(6[\theta-\Theta_6])\Big\rangle\\ &-6\Big\langle\tilde{\mathsf{v}}_{ij}\epsilon_{jk}\tilde{\mathsf{q}}_{ki}f(|\tilde{\mathsf{q}}|)\sin(6[\theta-\Theta_6])\Big\rangle\end{aligned} \tag{A54}$$

and into an equation characterizing the orientation:

$$\frac{\mathrm{d}\Theta_6}{\mathrm{d}t} = \Omega + \tilde{\mathsf{V}}_{ij}\epsilon_{jk}\tilde{\mathsf{Q}}_{ki}f(|\tilde{\mathsf{Q}}|) + \Sigma \tag{A55}$$

with correlations Σ given by:

$$\begin{aligned}\Sigma = \frac{1}{Z_6}\Bigg[&\frac{1}{6}\Big\langle \mathsf{v}_{kk}\sin(6[\theta-\Theta_6])\Big\rangle\\ &+\left(\Big\langle\omega\cos(6[\theta-\Theta_6])\Big\rangle - \Omega Z_6\right)\\ &+\Big(\Big\langle\tilde{\mathsf{v}}_{ij}\epsilon_{jk}\tilde{\mathsf{q}}_{ki}f(|\tilde{\mathsf{q}}|)\cos(6[\theta-\Theta_6])\Big\rangle\\ &\qquad - \tilde{\mathsf{V}}_{ij}\epsilon_{jk}\tilde{\mathsf{Q}}_{ki}f(|\tilde{\mathsf{Q}}|)Z_6\Big)\Bigg].\end{aligned} \tag{A56}$$

Eq. (A55) relates the orientation of the hexatic order Θ_6, which can be interpreted as an average triangle orientation, to the large-scale vorticity Ω. For what follows, we multiply Eq. (A55) with δt:

$$\delta\Psi = \delta\Theta_6 - \delta\tilde{\mathsf{U}}_{ij}\epsilon_{jk}\tilde{\mathsf{Q}}_{ki}f(|\tilde{\mathsf{Q}}|) - \Sigma\delta t. \tag{A57}$$

Here, $\delta\Theta_6$ denotes the change of the average triangle orientation Θ_6. Note the analogy of this equation with Eqs. (29) and (36).

To account for the effect of topological transitions, one can proceed as in Section IV. The displacement gradient across a topological transition is zero and so is its anisotropic part $\Delta\Psi = 0$ and the shear $\Delta\tilde{\mathsf{U}}_{ij} = 0$. To account for example for a T1 transition, we introduce a new term $\Delta\Xi_6^T$ into Eq. (A57), which represents the rotation by the T1 transition:

$$\Delta\Psi = \Delta\Theta_6 - \Delta\tilde{\mathsf{U}}_{ij}\epsilon_{jk}\tilde{\mathsf{Q}}_{ki}f(|\tilde{\mathsf{Q}}|) + \Delta\Xi_6^T. \tag{A58}$$

Here, $\Delta\Theta_6$ is the change of Θ_6 induced by the T1 transition, and we have set the correlations across the T1 transition to zero as we did in Section IV A. After all, we obtain from Eq. (A58) that $\Delta\Xi_6^T = -\Delta\Theta_6$.

Wrapping up, we find the following decomposition of the large-scale vorticity:

$$\Omega = \frac{\mathrm{d}\Theta_6}{\mathrm{d}t} - \tilde{\mathsf{V}}_{ij}\epsilon_{jk}\tilde{\mathsf{Q}}_{ki}f(|\tilde{\mathsf{Q}}|) + \Gamma_6^T + \Gamma_6^C + \Gamma_6^E - \Sigma \tag{A59}$$

with the rotations by T1 transitions Γ_6^T, cell divisions Γ_6^C, and cell extrusions Γ_6^E defined by:

$$\Gamma_6^T = -\sum_{k\in\mathrm{T1}} \Delta\Theta_6^k\,\delta(t-t_k) \tag{A60}$$

$$\Gamma_6^C = -\sum_{k\in\mathrm{CD}} \Delta\Theta_6^k\,\delta(t-t_k) \tag{A61}$$

$$\Gamma_6^E = -\sum_{k\in\mathrm{T2}} \Delta\Theta_6^k\,\delta(t-t_k). \tag{A62}$$

Here, the sums run over all topological transitions k of the respective kind, t_k denotes the time point of the respective transition, and $\Delta\Theta_6^k$ denotes the instantaneous change in Θ_6 induced by the transition.

Note that in principle, one could also use for instance the triatic order parameter:

$$P_3 = \Big\langle e^{3i\theta}\Big\rangle. \tag{A63}$$

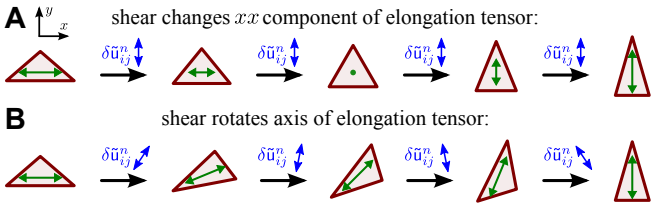

FIG. 16. Path-dependence of the cumulative pure shear. Shown are two finite deformations with the same initial and final states, but with a different cumulative shear. Initial and final states are isosceles triangles, with the same elongation norm. (A) The triangle is sheared along the y axis. (B) The triangle is sheared such that the elongation tensor is rotated but the norm stays constant.

However, for our purposes we prefer to use P_6 over P_3. This is because for a regular hexagonal array of cells, P_3 vanishes, whereas P_6 is nonzero. Hence, P_6 would allow us to track large-scale rotations of a regular hexagonal pattern of cells, which would not be possible using P_3.

9. Path-dependence of the cumulative pure shear

Here, we discuss the finite deformation of a triangular network that starts from a state with configuration I and ends in another state with configuration F. The initial and final configuration I and F respectively define all triangle corner positions and the topology of the network. We define the corresponding cumulative pure shear by:

$$\int_I^F \delta\tilde{\mathsf{U}}_{ij} = \int_0^T \tilde{\mathsf{V}}_{ij}\,\mathrm{d}t, \tag{A64}$$

where the deformation starts at time 0 in state I and ends at time T in state F.

The cumulative pure shear does not only depend on the initial and final states I and F, but also on the network states in between. We demonstrate this path-dependence of the cumulative pure shear for the case of a single triangle (Fig. 16). The initial state I is given by a triangle with an elongation tensor parallel to the x axis with $\tilde{\mathsf{q}}^n_{xx} = Q_0$, where Q_0 is a positive scalar. The final state F is given by a triangle with an elongation tensor parallel to the y axis with $\tilde{\mathsf{q}}^n_{xx} = -Q_0$. In initial and final states, the triangle areas are the same and in both states, $\theta^n = 0$. Fig. 16 illustrates two different deformation paths to reach state F from state I. In Fig. 16A, the triangle is sheared along the horizontal axis, which corresponds to an cumulative shear along this axis of:

$$\int_{\mathrm{A}} \delta\tilde{\mathsf{u}}^n_{xx} = -2Q_0. \tag{A65}$$

This follows from Eq. (19). In Fig. 16B, the triangle is undergoes a time-dependent pure shear such that the elongation axis is rotated but its norm stays constant. At the same time, to ensure that the orientation angle does not change $\delta\theta^n = 0$, the rotation $\delta\psi^n$ as given by Eq. (21) is nonzero. The additional contributions by the corotational term in Eq. (19) eventually yield [22]:

$$\int_{\mathrm{B}} \delta\tilde{\mathsf{u}}^n_{xx} = -\sinh(2Q_0). \tag{A66}$$

Thus, the cumulative pure shear for both integration paths is different – or put differently, the cumulative shear is path-dependent. Note that an equivalent statement is that the cumulative shear over a cyclic deformation is in general nonzero, where by *cyclic* deformation, we mean a deformation with coinciding initial and final states.

Finally, we remark that at least for a triangular network with more than two triangles, the path-dependence of the cumulative pure shear can be generalized as follows [22]. We consider a set of tensors G^{tr}_{ij}, G^{s}_{ijkl}, G^{a}_{ij}, and H_{ij} that only depend on the given state of the triangular network. Then, the following equation:

$$\int_I^F \left(G^{\mathrm{tr}}_{ij}\delta\mathsf{U}_{kk} + G^{s}_{ijkl}\delta\tilde{\mathsf{U}}_{kl} + G^{\mathrm{a}}_{ij}\delta\Psi\right) = H_{ij}(F) - H_{ij}(I) \tag{A67}$$

can be generally true only if $G^{s}_{ijkl} = 0$ and $G^{\mathrm{a}}_{ij} = 0$. Hence, even adding a state-dependent factor G^{s}_{ijkl} and including rotation and isotropic scaling does not resolve the general path-dependence of the cumulative pure shear.

Since any kind of two-dimensional material can be triangulated, path-dependence of the pure shear holds independent of our triangle-based approach. It is a mere consequence of integrating the instantaneous deformation rate V_{ij}, which is substantially different from defining deformation with respect to a fixed reference state as usually done in classical elasticity theory [33].

Appendix B: Analysis of experimental data

1. Quantification of spatially averaged cellular deformation contributions

The equations derived in Sections III B, III C, and V hold exactly only for infinitesimal deformations and time intervals. However, experimental data always has a finite acquisition frequency. Here, we discuss how we adapt our theoretical concepts to deal with finite time intervals in practice.

We start from a series O^k of observed states of a cellular network with $k = 1, \ldots, N_{\mathrm{states}}$. Each of these states defines cell center positions and cell neighborship relations. The states are registered at times t^k, respectively. We denote the corresponding time intervals by $\Delta t^k = t^{k+1} - t^k$. As a first step, each of the cellular network states is triangulated according to Section II D.

To quantify the deformation rate and all cellular contributions to it between two observed states O^k and O^{k+1}, we introduce three virtual intermediate network states I^k_1, I^k_2, and I^k_3 (Fig. 17, [6, 22]). By introducing these

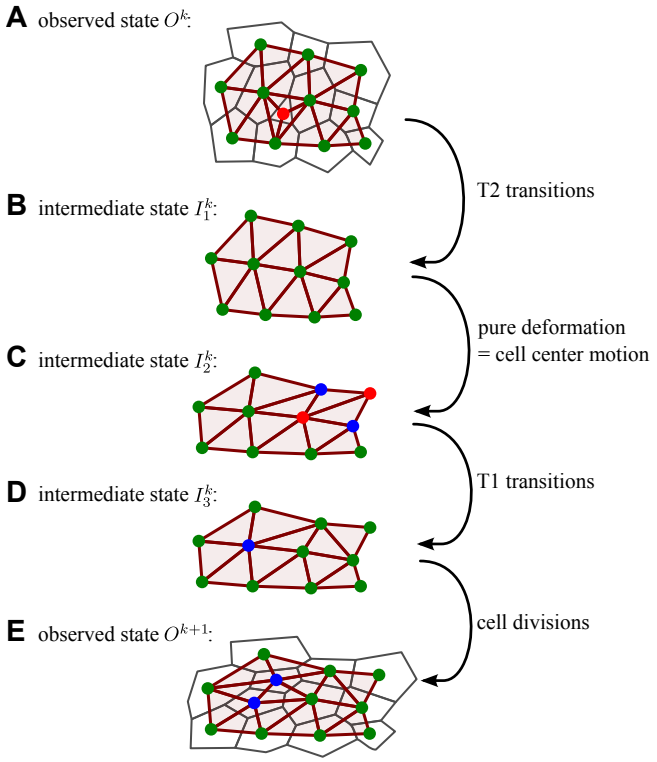

FIG. 17. Illustration of the virtual intermediate states I_1^k, I_2^k, and I_3^k introduced between two observed states O^k and O^{k+1}.

intermediate states, we shift all topological transitions to the beginning or to the end of the time interval Δt^k. This separates topological transitions from cell center motions, which now only occur between the states I_1^k and I_2^k (Fig. 17B,C). We justify this by the fact that given only the observed data, it is in principle impossible to know at what exact time between t^k and t^{k+1} a given topological transition occurred.

We define the three intermediate states I_1^k, I_2^k, and I_3^k based on the observed states O^k and O^{k+1} as follows.

1. The intermediate state I_3^k is defined based on O^{k+1} by reverting all divisions that occur between the observed states O^k and O^{k+1}. To this end, each pair of daughter cell centers is fused into a mother cell center. The position of the mother cell center is defined by the average position of the daughter cell centers.

2. The intermediate state I_1^k is defined based on O^k by removing the centers of all cells that undergo a T2 transition between the observed states O^k and O^{k+1}.

3. The intermediate states I_1^k and I_3^k contain the same set of cell centers, which however differ in their positions. Also, the topology of both states is different. We thus define the intermediate state I_2^k based on I_1^k by moving all cell centers to their respective positions in I_3^k.

Note that the intermediate states carry just enough information to define the triangulation. Vertex positions, which would be needed to define cellular networks are not contained.

For the precise explanation of how we compute the cellular contributions to the deformation rate, we focus on the pure shear part. Contributions to the isotropic expansion rate or the rotation rate can be computed analogously. In the following, we denote the large-scale shear rate quantified from experimental data and contributions to it with the superscript "exp".

We define the pure shear induced by a given kind of topological transition as the negative change of average elongation that is associated with the respective state change (Fig. 17). We thus compute the shear rates by T1 transitions $\tilde{\mathsf{T}}_{ij}^{\mathrm{exp}}$, cell divisions $\tilde{\mathsf{C}}_{ij}^{\mathrm{exp}}$, and T2 transitions $\tilde{\mathsf{E}}_{ij}^{\mathrm{exp}}$ as follows:

$$\tilde{\mathsf{T}}_{ij}^{\mathrm{exp}} = -\frac{1}{\Delta t^k}\Big[\tilde{\mathsf{Q}}_{ij}(I_3^k) - \tilde{\mathsf{Q}}_{ij}(I_2^k)\Big] \tag{B1}$$

$$\tilde{\mathsf{C}}_{ij}^{\mathrm{exp}} = -\frac{1}{\Delta t^k}\Big[\tilde{\mathsf{Q}}_{ij}(O^{k+1}) - \tilde{\mathsf{Q}}_{ij}(I_3^k)\Big] \tag{B2}$$

$$\tilde{\mathsf{E}}_{ij}^{\mathrm{exp}} = -\frac{1}{\Delta t^k}\Big[\tilde{\mathsf{Q}}_{ij}(I_1^k) - \tilde{\mathsf{Q}}_{ij}(O^k)\Big]. \tag{B3}$$

Here, $\tilde{\mathsf{Q}}_{ij}(X)$ denotes the average triangle elongation in the virtual or observed state X. We divide by the time interval Δt^k to obtain the respective rate of pure shear.

To compute the large-scale shear rate $\tilde{\mathsf{V}}_{ij}^{\mathrm{exp}}$, the corotational term $\tilde{\mathsf{J}}_{ij}^{\mathrm{exp}}$, and the correlation term $\tilde{\mathsf{D}}_{ij}^{\mathrm{exp}}$, we proceed as follows. We realized that direct application of Eq. (42) led to large deviations for the fly wing data, which is exact only to first order in the time interval Δt^k. We thus split the time interval Δt^k into N subintervals and then compute $\tilde{\mathsf{V}}_{ij}^{\mathrm{exp}}$, $\tilde{\mathsf{J}}_{ij}^{\mathrm{exp}}$, and $\tilde{\mathsf{D}}_{ij}^{\mathrm{exp}}$ by summing the respective subinterval contributions. To this end, we introduce intermediate states S^r with $r = 1, \ldots, N-1$, which are defined by interpolating all cell center positions linearly between the states $S^0 = I_1^k$ and $S^N = I_2^k$. Then, the velocity gradient tensor $\mathsf{V}_{ij}^{\mathrm{exp}}$ is computed by summing the deformation gradients defined by Eq. (11) for all subintervals:

$$\mathsf{V}_{ij}^{\mathrm{exp}} = \frac{1}{\Delta t^k}\sum_{r=0}^{N-1}\mathsf{U}_{ij}^r \tag{B4}$$

with the subinterval deformation gradient

$$\mathsf{U}_{ij}^r = -\frac{\epsilon_{im}}{2A(S^r)}\sum_{\alpha=1}^{M}\Big(r_m^{\alpha+1}(S^r) - r_m^{\alpha}(S^r)\Big)\times \Big(r_j^{\alpha+1}(S^{r+1}) + r_j^{\alpha}(S^{r+1}) - r_j^{\alpha+1}(S^r) - r_j^{\alpha}(S^r)\Big). \tag{B5}$$

Here, $A(S^r)$ and $\boldsymbol{r}^\alpha(S^r)$ are total triangulation area and position of the center of cell α in state S^r, respectively. The inner sum runs over all margin cells α in counterclockwise order. The shear rate $\tilde{\mathsf{V}}_{ij}$ is the symmetric, traceless part of V_{ij}.

The corotational term $\tilde{\mathsf{J}}_{ij}^{\text{exp}}$ is computed as follows:

$$\tilde{\mathsf{J}}_{ij}^{\text{exp}} = \sum_{r=0}^{N-1} \tilde{\mathsf{J}}_{ij}^{r} \tag{B6}$$

with

$$\tilde{\mathsf{J}}_{ij}^{r} = -2\Big[C^r \Psi^r + (1-C^r)(\Phi^{r+1} - \Phi^r)\Big]\epsilon_{ik}\tilde{\mathsf{Q}}_{kj}(S^r). \tag{B7}$$

Here, $C^r = \tanh(2|\tilde{\mathsf{Q}}^r|)/(2|\tilde{\mathsf{Q}}^r|)$, where $\tilde{\mathsf{Q}}_{kj}(S^r)$ is the average triangle elongation in state S^r, and $|\tilde{\mathsf{Q}}^r|$ and Φ^r are its norm and angle. The symbol Ψ^r denotes the antisymmetric part of the subinterval deformation tensor U_{ij}^r, analogous to Eq. (5).

The correlation term $\tilde{\mathsf{D}}_{ij}^{\text{exp}}$ is computed as

$$\tilde{\mathsf{D}}_{ij}^{\text{exp}} = \frac{1}{\Delta t^k}\sum_{r=0}^{N-1}\Bigg[-\Big(\Big\langle \mathsf{u}_{kk}^r \tilde{\mathsf{q}}_{ij}(S^r)\Big\rangle - \mathsf{U}_{kk}^r \tilde{\mathsf{Q}}_{ij}(S^r)\Big) + \Big(\langle \tilde{\mathsf{j}}_{ij}^r\rangle - \tilde{\mathsf{J}}_{ij}^r\Big)\Bigg] \tag{B8}$$

Here, $\mathsf{u}_{kk}^{n,r}$ and $\tilde{\mathsf{j}}_{ij}^{n,r}$ are isotropic expansion and corotational term of triangle n with respect to the subinterval between S^r and S^{r+1}, and $\tilde{\mathsf{q}}_{ij}^n(S^r)$ is the elongation of triangle n in state S^r. The averaging for a given value of the summation index r is carried out with respect to the triangle areas in state S^r.

Finally, we compute the corotational derivative of the average elongation as follows:

$$\frac{\mathrm{D}\tilde{\mathsf{Q}}_{ij}^{\text{exp}}}{\mathrm{D}t} = \frac{1}{\Delta t^k}\Big[\tilde{\mathsf{Q}}_{ij}(O^{k+1}) - \tilde{\mathsf{Q}}_{ij}(O^k) + \tilde{\mathsf{J}}_{ij}^{\text{exp}}\Big] \tag{B9}$$

Here, $\tilde{\mathsf{J}}_{ij}^{\text{exp}}$ is the corotational term as computed from Eq. (B6).

Using all these definitions, we can make Eq. (42) hold arbitrarily precise by choosing a sufficiently large value for N. For the data shown in Figs. 11 and 12, we chose $N = 100$. Note that this approach to deal with the finiteness of the time intervals Δt^k is different from the approaches chosen in our previous publications [6, 22].

2. Spatial patterns of shear components

To compute spatial patterns of large-scale tissue deformation and their cellular components as in Fig. 10, we introduce a grid of squared boxes, which are labeled by the index b. In Eq. (10), we introduced an average over triangles to compute large-scale quantities. Here, we introduce such an average for a given box b. For instance, the box-averaged shear rate $\tilde{\mathsf{V}}_{ij}^b = \langle \tilde{\mathsf{v}}_{ij}\rangle_b$ is defined as:

$$\langle \mathsf{v}_{ij}\rangle_b = \frac{1}{A_b}\sum_n a_b^n \mathsf{v}_{ij}^n \tag{B10}$$

The sum is over all triangles n that have an overlap with box b, and a_b^n is the area of this overlap. The normalization factor A_b is the overlap area between box b and the triangulation, i.e. $A_b = \sum_n a_b^n$.

Infinitesimal time intervals

Here and in the following, we focus our discussion on the computation of the pure shear part and its cellular contributions. First we ask how the box-averaged shear rate $\tilde{\mathsf{V}}_{ij}^b$ decomposes into cellular contributions for an infinitesimal time interval δt and in the absence of topological transitions. To this end, we insert the relation between single triangle shear rate and triangle shape, Eq. (23), into Eq. (B10) and obtain an equation that is analogous to Eq. (32):

$$\tilde{\mathsf{V}}_{ij}^b = \frac{\mathrm{D}\tilde{\mathsf{Q}}_{ij}^b}{\mathrm{D}t} + \tilde{\mathsf{D}}_{ij}^b. \tag{B11}$$

However here, the corotational time derivative contains an additional term $\tilde{\mathsf{B}}_{ij}^b$:

$$\frac{\mathrm{D}\tilde{\mathsf{Q}}_{ij}^b}{\mathrm{D}t} = \frac{\delta\tilde{\mathsf{Q}}_{ij}^b}{\delta t} + \tilde{\mathsf{B}}_{ij}^b + \frac{\delta\tilde{\mathsf{J}}_{ij}^b}{\delta t} \tag{B12}$$

with the definitions

$$\tilde{\mathsf{Q}}_{ij}^b = \langle \tilde{\mathsf{q}}_{ij}\rangle_b \tag{B13}$$

$$\tilde{\mathsf{B}}_{ij}^b = -\left(\left\langle \tilde{\mathsf{q}}_{ij}\frac{\mathrm{d}}{\mathrm{d}t}(\ln f_b)\right\rangle_b - \tilde{\mathsf{Q}}_{ij}^b\left\langle \frac{\mathrm{d}}{\mathrm{d}t}(\ln f_b)\right\rangle_b\right) \tag{B14}$$

$$\delta\tilde{\mathsf{J}}_{ij}^b = -2\Big[C_b\langle\delta\psi\rangle_b + (1-C_b)\delta\Phi_b\Big]\epsilon_{ik}\tilde{\mathsf{Q}}_{kj}^b. \tag{B15}$$

Here, $f_b^n = a_b^n/a^n$ is the area fraction of triangle n that is inside box b, and $C_b = \tanh(2|\tilde{\mathsf{Q}}^b|)/2|\tilde{\mathsf{Q}}^b|$. The symbols $|\tilde{\mathsf{Q}}^b|$ and Φ_b denote norm and angle of the average elongation tensor $\tilde{\mathsf{Q}}_{ij}^b$, respectively. The correlation term in Eq. (B11) is defined by

$$\tilde{\mathsf{D}}_{ij}^b = -\Big(\big\langle \mathsf{v}_{kk}\tilde{\mathsf{q}}_{ij}\big\rangle_b - \langle \mathsf{v}_{kk}\rangle_b\tilde{\mathsf{Q}}_{ij}^b\Big) + \frac{1}{\delta t}\Big(\langle\delta\tilde{\mathsf{j}}_{ij}\rangle_b - \delta\tilde{\mathsf{J}}_{ij}^b\Big). \tag{B16}$$

Eq. (32) describes a triangulation that is followed as it moves through space, whereas here, we consider a box b that is fixed in space. Correspondingly, the we interpret the additional term $\tilde{\mathsf{B}}_{ij}^b$ in the corotational derivative as a convective term.

Finite time intervals

To practically compute the pure shear contributions for a given box b for experimental image data, we proceed similar to the previous section. We consider again a finite time interval Δt^k between two subsequent observed states O^k and O^{k+1}. To separate pure shear contributions by topological transitions from contributions by cell

center motion, we introduce again the intermediate states illustrated in Fig. 17. Correspondingly, the shear rates by T1 transitions $\tilde{\mathsf{T}}_{ij}^{\mathrm{exp},b}$, by cell divisions $\tilde{\mathsf{C}}_{ij}^{\mathrm{exp},b}$, and by T2 transitions $\tilde{\mathsf{E}}_{ij}^{\mathrm{exp},b}$ are defined as:

$$\tilde{\mathsf{T}}_{ij}^{\mathrm{exp},b} = -\frac{1}{\Delta t^k}\Big[\tilde{\mathsf{Q}}_{ij}^b(I_3^k) - \tilde{\mathsf{Q}}_{ij}^b(I_2^k)\Big] \tag{B17}$$

$$\tilde{\mathsf{C}}_{ij}^{\mathrm{exp},b} = -\frac{1}{\Delta t^k}\Big[\tilde{\mathsf{Q}}_{ij}^b(O^{k+1}) - \tilde{\mathsf{Q}}_{ij}^b(I_3^k)\Big] \tag{B18}$$

$$\tilde{\mathsf{E}}_{ij}^{\mathrm{exp},b} = -\frac{1}{\Delta t^k}\Big[\tilde{\mathsf{Q}}_{ij}^b(I_1^k) - \tilde{\mathsf{Q}}_{ij}(O^k)^b\Big]. \tag{B19}$$

The tensors $\tilde{\mathsf{Q}}_{ij}^b(X)$ denote the box-averaged triangle elongation in the virtual or observed state X.

To compute the box-averaged shear rate $\tilde{\mathsf{V}}_{ij}^{\mathrm{exp},b}$, the convective term $\tilde{\mathsf{B}}_{ij}^{\mathrm{exp},b}$, the corotational term $\tilde{\mathsf{J}}_{ij}^{\mathrm{exp},b}$, and the correlations $\tilde{\mathsf{D}}_{ij}^{\mathrm{exp},b}$ between O^k and O^{k+1}, we use the subintervals and the states S^r with $r = 0,\dots,N$ introduced in the previous section. We again compute the quantities for each subinterval separately and then sum over the subintervals:

$$\tilde{\mathsf{V}}_{ij}^{\mathrm{exp},b} = \frac{1}{\Delta t^k}\sum_{r=0}^{N-1}\langle\tilde{\mathsf{u}}_{ij}^r\rangle \tag{B20}$$

$$\tilde{\mathsf{B}}_{ij}^{\mathrm{exp},b} = -\frac{1}{\Delta t^k}\sum_{r=0}^{N-1}\Bigg(\Big\langle\tilde{\mathsf{q}}_{ij}(S^r)\frac{\Delta f_b^r}{f_b^r}\Big\rangle_b - \tilde{\mathsf{Q}}_{ij}^b(S^r)\Big\langle\frac{\Delta f_b^r}{f_b^r}\Big\rangle_b\Bigg) \tag{B21}$$

$$\tilde{\mathsf{J}}_{ij}^{\mathrm{exp},b} = \sum_{r=0}^{N-1}\tilde{\mathsf{J}}_{ij}^{b,r} \tag{B22}$$

$$\tilde{\mathsf{J}}_{ij}^{b,r} = -2\Big[C^{b,r}\Psi^{b,r} + (1-C^{b,r})(\Phi^{b,r+1}-\Phi^{b,r})\Big]\times \epsilon_{ik}\tilde{\mathsf{Q}}_{kj}^b(S^r) \tag{B23}$$

$$\tilde{\mathsf{D}}_{ij}^{\mathrm{exp},b} = \frac{1}{\Delta t^k}\sum_{r=0}^{N-1}\Bigg[-\Big(\big\langle\mathsf{u}_{kk}^r\tilde{\mathsf{q}}_{ij}(S^r)\big\rangle_b - \langle\mathsf{u}_{kk}^r\rangle_b\tilde{\mathsf{Q}}_{ij}^b(S^r)\Big) + \Big(\langle\tilde{\mathsf{j}}_{ij}^r\rangle_b - \tilde{\mathsf{J}}_{ij}^{b,r}\Big)\Bigg]. \tag{B24}$$

Here, $\mathsf{u}_{kk}^{n,r}$ and $\tilde{\mathsf{u}}_{ij}^{n,r}$ are trace and symmetric, traceless part of the deformation tensor of triangle n according to Eq. (8) with respect to the subinterval between S^r and S^{r+1}, $\tilde{\mathsf{q}}_{ij}^n(S^r)$ is the elongation of triangle n in state S^r, $f_b^{n,r}$ is the value of f_b^n in state S^r, and its change is $\Delta f_b^{n,r} = f_b^{n,r+1} - f_b^{n,r}$. We furthermore used $C^{b,r} = \tanh(2|\tilde{\mathsf{Q}}^{b,r}|)/(2|\tilde{\mathsf{Q}}^{b,r}|)$, where $|\tilde{\mathsf{Q}}^{b,r}|$ and $\Phi^{b,r}$ are norm and angle of the box-averaged elongation in state S^r, $\tilde{\mathsf{Q}}_{ij}^b(S^r)$. The symbol $\Psi^{b,r}$ denotes the antisymmetric part of the box-averaged deformation tensor in state r and the tensor $\tilde{\mathsf{j}}_{ij}^{n,r}$ denotes the corotational term for triangle n with respect to the subinterval between S^r and S^{r+1}. Finally, the corotational derivative of the box-averaged elongation is computed as

$$\frac{\mathrm{D}\tilde{\mathsf{Q}}_{ij}^{\mathrm{exp},b}}{\mathrm{D}t} = \frac{1}{\Delta t^k}\Big[\tilde{\mathsf{Q}}_{ij}^b(O^{k+1}) - \tilde{\mathsf{Q}}_{ij}^b(O^k) + \tilde{\mathsf{J}}_{ij}^{\mathrm{exp},b}\Big]. \tag{B25}$$

For the patterns shown in Fig. 10, we used $N = 100$ subintervals.

Appendix C: Comparison to related approaches

Other work has discussed tissue deformation and contributions of cellular processes to tissue deformation [13–18]. Such approaches differ in the definitions of cellular contributions to tissue shear as well as the tissue deformation measures used. Our approach provides an exact local decomposition of tissue deformation into cellular contributions which can be coarse-grained by simple averaging (Eq. (3)). In fact, an area-weighted average of triangle measures generates in our approach the exact large scale deformation tensor (Eq. (9)). Other approaches are usually either approximate and neglect certain contributions or they involve nonlinear deformation measures, which cannot be simply averaged to obtain the large-scale tissue deformation. However in our approach, averaging of corotational terms leads to correlation contributions that are exactly defined and correspond to a renormalization effect. Note that the definitions of deformations and deformation contributions defined here commute with their coarse-graining. This implies that if a cell network is divided into subnetworks, our results are independent of whether (i) the deformation and its contributions are determined for the whole tissue or (ii) the deformations and their respective contributions are determined first for each subnetwork individually and the resulting quantities are then averaged. This property holds at most approximately for alternative approaches that use nonlinearities [14, 18]. Furthermore, in the work presented here, large-scale tissue deformation can be determined from the deformation of the tissue margin alone (Eqs. (4) and (11)). Note that because of these coarse-graining properties, we could identify the significance of correlation contributions to tissue shear in the developing fly wing (Eq. (34)).

Our approach can separate the precise contributions of different types of topological transitions to tissue shear. Recent work also has this property [18], but another, qualitatively different, approach currently does not provide such a separation [15, 16]. The approach in Refs. [15, 16] accounts for cell rearrangements (i.e. T1 transitions) by a tensor that quantifies the continuous sliding of cells relative to each other. As a consequence, the deformation contribution of a T1 transition to tissue shear is not associated with the precise time point of the topological transition, but is typically distributed over a short time interval. In contrast, the method of Ref. [18] and the Triangle Method presented here associate the contribution of a topological transition to deformations with the time point at which the transition occurs. There

exists an analogy of tissue deformations to plasticity of complex materials. Cell deformations correspond to elastic material deformations and topological transitions correspond to changes of a stress-free reference state of a plastic material. Both elastic and plastic stress events contribute to the overall material deformation. Plastic contributions are associated with the time points when the reference state defining elastic stresses changes. The precise definition of such reference state changes permits the exact decomposition of overall deformations in contributions stemming from specific reference changes.

In the main text of our manuscript, we have developed our framework for the case of infinitesimal time intervals. However, our approach can also be applied to finite time intervals as discussed in Appendix B 1. The essential idea is to integrate the infinitesimal quantities over the finite time interval. When in experiments only network configurations at discrete time points are available, this can be done by linearly interpolating the cell positions between frames. Alternative approaches decompose finite tissue deformations in a non-linear manner which does not require this interpolation [13, 18]. Note that the equations presented in the main text are valid for infinitesimal time intervals between subsequent states. However, they hold for arbitrary cell shapes.

The frameworks based on infinitesimal time intervals, in Refs. [14–16] and in our work, have the property that contributions of cell shape changes to tissue deformations can be expressed as a difference or a material time derivative of a state quantity (Eqs. (23), (32), and (42)). This directly reflects the fact that cellular shape only depends on the geometry of a tissue at a given time point. This property is somewhat obscured in approaches that use nonlinearities to account for finite time intervals [18].

[1] L. Wolpert, R. Beddington, T. M. Jessell, P. Lawrence, E. M. Meyerowitz, and J. Smith, *Principles of Development* (Oxford University Press, 2001).

[2] J. T. Blankenship, S. T. Backovic, J. S. Sanny, O. Weitz, and J. a. Zallen, Developmental Cell **11**, 459 (2006).

[3] B. Aigouy, R. Farhadifar, D. B. Staple, A. Sagner, J.-C. Röper, F. Jülicher, and S. Eaton, Cell **142**, 773 (2010).

[4] F. Bosveld, I. Bonnet, B. Guirao, S. Tlili, Z. Wang, A. Petitalot, R. Marchand, P.-L. Bardet, P. Marcq, F. Graner, and Y. Bellaiche, Science **336**, 724 (2012).

[5] M. Merkel, A. Sagner, F. S. Gruber, R. Etournay, C. Blasse, E. Myers, S. Eaton, and F. Jülicher, Current Biology **24**, 2111 (2014).

[6] R. Etournay, M. Popović, M. Merkel, A. Nandi, C. Blasse, B. Aigouy, H. Brandl, G. Myers, G. Salbreux, F. Jülicher, and S. Eaton, eLife **4**, e07090 (2015).

[7] P. J. Keller, A. D. Schmidt, J. Wittbrodt, and E. H. Stelzer, Science **322**, 1065 (2008).

[8] R. Etournay, M. Merkel, M. Popović, H. Brandl, N. A. Dye, B. Aigouy, G. Salbreux, S. Eaton, and F. Jülicher, eLife **5** (2016), 10.7554/eLife.14334.

[9] V. Wiesmann, D. Franz, C. Held, C. Münzenmayer, R. Palmisano, and T. Wittenberg, Journal of microscopy **257**, 39 (2015).

[10] K. R. Mosaliganti, R. R. Noche, F. Xiong, I. a. Swinburne, and S. G. Megason, PLoS Computational Biology **8**, e1002780 (2012).

[11] P. Barbier de Reuille, A.-L. Routier-Kierzkowska, D. Kierzkowski, G. W. Bassel, T. Schüpbach, G. Tauriello, N. Bajpai, S. Strauss, A. Weber, A. Kiss, A. Burian, H. Hofhuis, A. Sapala, M. Lipowczan, M. B. Heimlicher, S. Robinson, E. M. Bayer, K. Basler, P. Koumoutsakos, A. H. Roeder, T. Aegerter-Wilmsen, N. Nakayama, M. Tsiantis, A. Hay, D. Kwiatkowska, I. Xenarios, C. Kuhlemeier, and R. S. Smith, eLife **4**, e05864 (2015).

[12] R. Cilla, V. Mechery, B. Hernandez de Madrid, S. Del Signore, I. Dotu, and V. Hatini, PLOS Computational Biology **11**, e1004124 (2015).

[13] G. W. Brodland, D. I. L. Chen, and J. H. Veldhuis, International Journal of Plasticity **22**, 965 (2006), arXiv:31144461582.

[14] F. Graner, B. Dollet, C. Raufaste, and P. Marmottant, The European Physical Journal E **25**, 349 (2008).

[15] G. B. Blanchard, A. J. Kabla, N. L. Schultz, L. C. Butler, B. Sanson, N. Gorfinkiel, L. Mahadevan, and R. J. Adams, Nature Methods **6**, 458 (2009).

[16] A. Kabla, G. Blanchard, R. Adams, and L. Mahadevan, in *Cell Mechanics: From Single Scale-Based Models to Multiscale Modeling* (2010) pp. 351–377.

[17] A. D. Economou, L. J. Brock, M. T. Cobourne, and J. B. a. Green, Development **140**, 4740 (2013).

[18] B. Guirao, S. U. Rigaud, F. Bosveld, A. Bailles, J. López-Gay, S. Ishihara, K. Sugimura, F. Graner, and Y. Bellaïche, eLife **4** (2015), 10.7554/eLife.08519.

[19] The polygonal network is introduced just for the sake of clarity here. All of our results are equally applicable for a much broader class of cellular networks where cell outlines may be curved.

[20] As long as the initial triangle has nonzero area.

[21] This is because from Eqs. (6) and (8) follows that if Eq. (7) holds for one corner of n, it also holds for the other two corners.

[22] M. Merkel, *From cells to tissues: Remodeling and polarity reorientation in epithelial tissues*, Ph.D. thesis, Technische Universität Dresden (2014).

[23] Note that Eq. (15) defines the triangle orientation angle θ modulo $2\pi/3$, because of the different possible associations of the corners of the reference triangle to the corners of triangle n. We require the associations between the triangle corners to be made going around both triangles in the same order – either clockwisely or counterclockwisely.

[24] R. B. Bird, O. Hassager, R. C. Armstrong, and C. F. Curtiss, *Dynamics of polymeric liquids, Volume 2: Kinetic Theory*, 2nd ed. (Wiley, New York, 1987).

[25] For such an average, the cellular quantities $\tilde{\mathsf{q}}^\alpha_{ij}$ and $\tilde{\mathsf{v}}^\alpha_{ij}$ have to be weighted by the summed area $a^\alpha_\triangle = \sum_n a^n$ of all triangles n belonging to the respective cell α. Up to boundary terms these averages then respectively correspond to the large-scale quantities $\tilde{\mathsf{Q}}_{ij}$ and $\tilde{\mathsf{V}}_{ij}$.

[26] More precisely, here and in the following, we consider

topological transitions occurring in bulk. For a discussion of topological transitions occurring at the margin of the polygonal network, i.e. topological transitions altering the sequence of cell centers that forms the margin of the triangulation, see [22].
[27] Note that this is a convention and that different choices are possible as well (see Appendix A 6).
[28] T. Bittig, O. Wartlick, A. Kicheva, M. González-Gaitán, and F. Jülicher, New Journal of Physics **10**, 063001 (2008).
[29] J. Ranft, M. Basan, J. Elgeti, J.-F. Joanny, J. Prost, and F. Julicher, Proceedings of the National Academy of Sciences **107**, 20863 (2010).
[30] See Supplemental Material at [URL will be inserted by publisher].
[31] See Supplemental Material at [URL will be inserted by publisher].
[32] See Supplemental Material at [URL will be inserted by publisher].
[33] L. D. Landau and E. M. Lifshitz, *Pergamon Press*, Vol. 7 (1970) pp. 438–442.